A BULK-FLOW MODEL OF MULTIPLE BLADE, MULTIPLE POCKET GAS DAMPER SEALS

by

Jiming Li
Dr. Luis San Andrés

May 1998

TRC-SEAL-9-98

Texas A&M University
Mechanical Engineering Department

A BULK-FLOW MODEL OF MULTIPLE BLADE, MULTIPLE POCKET GAS DAMPER SEALS

Jiming Li,
Research Assistant

Principal Investigator
Luis San Andrés

May 1998

A Research Progress Report to the
Turbomachinery Research Consortium

A Bulk-Flow Model of Multiple-Blade, Multiple Pocket Gas Damper Seals

TABLE OF CONTENTS

A Bulk-Flow Model of Multiple Blade, Multiple Pocket Gas Damper Seals

Jiming Li and Luis San Andrés

Executive Summary

A bulk-flow model for determination of the dynamic force and sealing characteristics of multiple-blade, multiple-pocket gas damper seals is presented. Zeroth- and first-order equations describe the centered seal equilibrium flow and the perturbed flow for small amplitude rotor motions. The one-control volume model considers the circumferential flow within the seal cavity (or pockets), the flow across the radial baffles and the mass flow rates through the blade tips. Flow turbulence is accounted for with turbulent shear stress parameters and Moody's friction factors in the circumferential bulk-flow momentum equation. The effects of the radial baffles' thickness and clearance on decelerating the swirl flow are of importance for a proper analysis of pocket damper seals. The zeroth- and first-order flow equations are solved numerically using a robust *CFD* method. A PC FORTRAN program computes the seal leakage, cavity pressures and dynamic force coefficients as a function of the seal geometry and operating conditions. Theoretical predictions from the bulk-flow model and an earlier (simplified) model are compared to flow rates and rotordynamic force coefficients for two multiple-pocket gas damper seals tested at the Laboratory. The comparisons illustrate that the current bulk-flow model predicts reasonably well the leakage and dynamic force coefficients of multiple-tooth, multiple-pocket gas damper seals.

The literature on leakage models for brush seals is reviewed. A simple computational model for evaluation of the leakage trough brush seals is derived from a published description. This model will be incorporated next year to extend the current bulk flow model for analysis of hybrid seals, i.e. labyrinth or pocket damper seals with a brush seal installed at the seal discharge plane.

NOMENCLATURE

A $L(B+H)$, cross-section area of the seal cavity [m^2]
B height of the seal teeth [m]
C_{ij} damping coefficients [N-s/m], $i, j = X, Y$
D_h $2L(B+H)/(L+B+H)$, hydraulic diameter [m]
e_X, e_Y rotor center displacements in the X and Y directions [m]
e_r, e_s mean roughness at rotor and stator surfaces [m]
H seal clearance [m]
H_w gap between the baffle tip and rotor surface [m]
K_{ij} stiffness coefficients [N/m], $i, j = X, Y$
L axial length of seal pocket [m]
$\dot{M}$ axial mass flow rate [kg/m-s]
N_c number of circumferential pockets in one axial cavity
N_w number of seal axial cavities
P fluid pressure in seal pocket [N/m^2]
P_b back pressure at seal exit [N/m^2]
P_s supply pressure at seal inlet [N/m^2]
P_w fluid pressure at the baffle [N/m^2]
R_a $(R_r+R_s)/2$, average seal radius [m]
R_g gas constant [J/kg-°K]
R_r rotor radius [m]
R_s seal outer radius [m]
Re_r $\rho D_h[(U-\Omega R_r)^2+W^2]^{1/2}/\mu$, local Reynolds number at the rotor surface
Re_s $\rho D_h(U^2+W^2)^{1/2}/\mu$, local Reynolds number at the stator surface
Re_p $(\rho_* V_* L_*/\mu_*)$, reference flow Reynolds number
Re_c $Re_p (L_*/R_r)$, modified reference flow Reynolds number
Re_t $Re_p (L_*/R_r)\sigma$, nominal squeeze film Reynolds number
S baffle thickness between pockets [m]
T gas temperature [°K]
U circumferential bulk-flow velocity in seal pocket [m/s]
U_s $\alpha\Omega R_r$, pre-swirl velocity of gas flow at seal inlet [m/s]
U_w circumferential velocity of gas flow at the baffle [m/s]
V_* $(R_g T)^{1/2}$, characteristic speed of gas [m/s]
W axial bulk-flow velocity [m/s]
f_r, f_s $a_m[1 + [c_m e_{r,s}/(B+H) + b_m/Re_{r,s}]^{em}]$ Moody's friction factors at the rotor and stator surfaces
$a_m=0.001375$; $b_m=10^6$; $c_m=10^4$; $e_m=1/3$
k_r, k_s $f_{r,s}Re_{r,s}$, turbulent shear stress parameters at the rotor and stator surfaces
k_J, k_x $\zeta_r k_r$, $(\zeta_r k_r)/2+(\zeta_r L+B_s+B_s)k_s/2L$, dimensionless shear

stress factors

α inlet pre-swirl velocity ratio

μ_c "kinetic-energy carryover" factor of gas flow across seal teeth

μ_f gas flow coefficient across seal teeth

τ ωt, time coordinate

$\Delta\tau_x$ $-(k_x U - k_f \Omega R_r/2)(\mu L/D_h)$, shear stress difference from seal stator and rotor surfaces

ζ_r $R_r / R_a = 2 / (1+R_s / R_r)$

ζ_s $R_s / R_a = 2 / (1+R_r / R_s)$

ξ_w loss coefficient at the baffle

Λ $\Omega R_r/V_*$, rotor surface speed parameter

σ $\omega R_r/V_*$, excitation frequency parameter

ρ gas density [kg/m^3]

μ gas viscosity [N-s/m^2]

γ ratio of gas specific heats

Ω angular speed of rotor [rad/s]

ω angular whirling frequency of the rotor [rad/s]

Subscripts:

0 zeroth-order variable

i variable in the i_{th} cavity

j first-order variable

s seal upstream

b seal downstream

u local upstream

d local downstream

w baffle wall

$*$ characteristic values

1. INTRODUCTION

1.1 LABYRINTH SEALS AND THEIR EFFECT ON ROTORDYNAMICS

Labyrinth seals are widely used as balance drum, interstage and impeller eye seals to restrict leakage flow rate through rotor-stator clearances from a high-pressure region to a low-pressure region. Since in most cases, labyrinth seals are not located at shaft vibration nodes, they potentially have a more significant impact than bearings or bearing dampers on the dynamic characteristics of compressors and turbines. Labyrinth seals have been confirmed to be a major source of destabilizing forces resulting in rotordynamic instability problems (Pollmann and Termuehlen, 1975, Greathead and Bostow, 1976, Doyle, 1980, and Gelin, et al., 1996). On the other hand, a damper seal or squeeze film bearing damper acting directly at the center of the rotor would be most efficient in improving the rotordynamic stability of rotor-bearing systems (Lund, 1974). Childs and Vance (1997) summarize the latest advances is gas seals and detail their influence on the dynamics of turbines and compressors.

Seal forces are in general functions of the fluid properties, operating conditions and geometric configuration. For small amplitudes of rotor motion (X, Y) about an equilibrium position, these forces $(F_i)_{i=X,Y}$ are typically represented as linearized stiffness $(K_{i,j})_{i,j=X,Y}$ and damping $(C_{i,j})_{i,j=X,Y}$ force coefficients (Childs, 1993),

$$\begin{bmatrix} F_X \\ F_Y \end{bmatrix} = \begin{bmatrix} K_{XX} & K_{XY} \\ K_{YX} & K_{YY} \end{bmatrix} \begin{bmatrix} X \\ Y \end{bmatrix} + \begin{bmatrix} C_{XX} & C_{XY} \\ C_{YX} & C_{YY} \end{bmatrix} \begin{bmatrix} \dot{X} \\ \dot{Y} \end{bmatrix} \qquad (1)$$

Accurate seal force coefficients are necessary to predict correctly the critical speeds and dynamic stability of rotor/bearing/seal systems. From a rotordynamics point of view, large positive direct damping (C_{XX}, C_{YY}) and small or null cross-coupled stiffness (K_{XY}, K_{YX}) are desired to suppress rotor vibration and to enhance the dynamic stability in high performance of turbomachinery.

Vance and Schultz (1993) introduce a novel type of multiple-pocket gas damper seal derived from conventional teeth-on-stator labyrinth seals. This type of gas damper seal is an attractive alternative to conventional labyrinth seals since it provides significantly more direct damping. The first field application of the seal has demonstrated the dynamic forced performance of the seal damper to be much better than that of conventional labyrinth seals (Richards, et al., 1995).

In practice, a multiple-pocket, multiple-teeth gas damper seal consists of several two-bladed, damper cavity modules and two-bladed, labyrinth cavity modules stacked axially as shown in Figure 1. The two-bladed damper cavity module has radial baffles which divide the circumferential groove into several identical pockets, whereas a two-bladed labyrinth cavity module has one single annular groove. A pocket damper cavity module has two distinct features that are critical in providing damping. First, the radial rotor to blade clearances must diverge in the direction of axial flow; and second, the fixed radial baffles retard the development of the circumferential flow in the seal pocket.

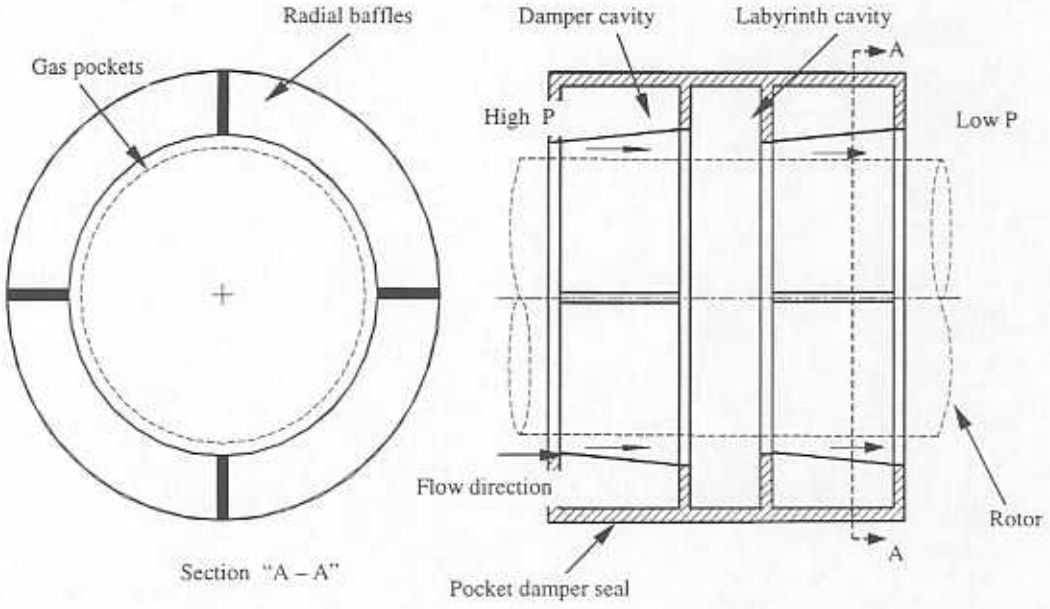

Figure 1. Schematic of a four-tooth, four-pocket gas damper seal

1.2 Background and State of the Art on Gas Pocket Damper Seals

Since the early 1980's, numerous investigations have been carried out to achieve stable annular gas seal configurations based on the following desired features:

- To reduce the magnitude and change the direction of the cross-coupled stiffness coefficients by retarding the development of the circumferential flow in the seal, and,
- To provide large positive direct damping.

Benckert and Wachter (1980) present an early comprehensive experimental investigation of the flow-induced forces in gas labyrinth seals. The measurements show that the circumferential flow causes an unsymmetrical pressure distribution in off centered labyrinth seals. The tests demonstrate that the cross-coupled stiffness coefficients depend strongly on the gas pre-swirl velocity. However, no damping coefficients are available from these static tests.

Childs and Scharrer (1986a and 1988) perform extensive experiments to measure the rotordynamic coefficients for two types of see-through labyrinth seals. One is a teeth-on-rotor seal (TOR) and the other is a teeth-on-stator seal (TOS). The seal stiffness and damping coefficients are identified from measured mechanical impedances. Measurements show that the test labyrinth seals have small positive direct damping coefficients. Typically, direct stiffness and damping coefficients are sensitive to the supply pressure and the inlet tangential velocity, but insensitive to the rotor speed.

Murphy and Vance (1980) extend *Alford's theory* (Alford, 1965) to a multiple-bladed labyrinth seal while neglecting the circumferential flow within the seal. The model predicts a ten-blade diverging clearance labyrinth seal of large diameter (200 mm) and at a working pressure ratio[1] equal to 10 can have a direct damping coefficient equal to 87,560 N-s/m, which is about the same order of magnitude as that generated by a squeeze film bearing damper of similar dimensions. Vance, et al. (1993a) conduct extensive coast-down experiments to evaluate the equivalent damping characteristics of labyrinth seals. Both teeth-on-stator and teeth-on-rotor gas labyrinth seals are tested

[1] The pressure ratio is defined as the ratio of seal inlet feed pressure to the exit or discharge pressure.

with different clearance configurations. However, the experimental results demonstrate that the equivalent damping coefficient from various types of labyrinth gas seals is generally very small. At a pressure ratio of 10, the measured equivalent damping coefficient is only equal to 876 N-s/m for a twelve bladed, straight TOR labyrinth seal of 173 mm diameter and 102 mm length.

Inlet swirl control, an effective method to improve seal rotordynamic stability, retards or eliminates the circumferential flow in labyrinth seal cavities. Benckert and Wachter (1980) verify experimentally that the cross-coupled force of a TOS gas labyrinth seal is reduced dramatically after installing a swirl brake at the entrance to the labyrinth seal, and thus reducing the positive pre-swirl velocity. Later, the effectiveness of the swirl brake technology is further demonstrated for various TOR gas labyrinth seals (Childs and Ramsey, 1991, Kwanka, 1997). The anti-swirl injection technology also has been successfully utilized to eliminate sub-synchronous vibration in industrial compressors (Zhou, 1986, and Fozi, 1986). The gas injected at an angle breaks up the circumferential swirl flow or may even change the circumferential flow direction in the seal. Some manufactures have implemented this technique to enhance the rotordynamic performance and reliability in a compressor (Kanki, et al. 1988).

There are few ways to enhance the damping characteristic of gas labyrinth seals. Childs et al. (1989) compare the rotordynamic coefficients of long honeycomb-stator seals (L = 50.8 mm) to those of a TOS labyrinth seal. A smooth rotor of 150.54 mm diameter is used in the tests. The measurements show that the honeycomb-stator/smooth-rotor seals have a larger positive direct damping coefficient while their cross-coupled stiffness coefficients are comparable to those of the labyrinth seal. However, the honeycomb-stator is not an effective mean to improve the rotordynamic stability of tooth-on-rotor (TOR) labyrinth seals (Hawkins et al., 1989, Kwanka, 1997). Childs and Kleynhans (1993) verify experimentally that short honeycomb stator seals (L<25.4 mm) can not be categorized as "damper seals" since their damping coefficients are not larger than those from smooth-stator seals and labyrinth seals.

Yu and Childs (1997) test a hole-pattern-stator gas damper seal. This type of seal is easier to fabricate than a honeycomb seal. The experiments show that the hole-pattern-stator gas damper seal provides higher effective damping and a reduced leakage rate (-12%) when compared to a conventional honeycomb seal. Therefore, the hole-pattern-stator gas damper seal may become a more favorable alternative design to honeycomb seals.

Vance, et al. (1993b) introduce a gas pocket damper actuator as a viable replacement to oil squeeze film dampers in high temperature turbomachinery applications. The dynamic gas pressure in a pocket can be out of phase with the vibratory motion since the vibratory motion regulates the gas flow into and out of the pocket through orifice like restrictions. Therefore, the gas pocket actuator may work like an ideal damper element. An isentropic flow (ideal fluid) model predicts dynamic force coefficients proportional to the supply pressure though strongly dependent on the excitation frequency. A positive damping action occurs if the inlet restriction varies dynamically with the rotor motion. The theory also predicts that the characteristic of damping is determined by the dynamic variation of the ratio of inlet area to exit area in the damper. For best results, the outlet or discharge flow restriction must remain insensitive to the vibratory motion.

Sundararajan and Vance (1993a) improve the model developed by Vance, et al. (1993b) by including the effects of the supply groove, the dynamic variations of the inlet feeding holes and flow choking on the dynamic performance of the gas pocket damper actuator. Sundararajan and Vance (1993b) confirm experimentally that the test pocket gas damper actuator could provide a maximum damping of 2,310 N-sec/m (13.2 lb-sec/in) at an exciting frequency of 100 Hz for a pressure drop of 4.13 bars.

By using the same physical mechanism as in the gas pocket damper actuator, Vance and Schultz (1993) introduce a novel type of gas damper seal that has a diverging clearance configuration and circumferential pockets. Rigid radial baffles effectively reduce the mean circumferential bulk-flow velocity in the seal cavities. The pocket gas damper seal, unlike other damping devices commonly used in turbomachinery, does not

rely solely on the fluid viscosity to dissipate energy. The first tests of a two-bladed prototype in a nonrotating rig show that the seal has 15 times more effective damping than a conventional labyrinth seal (Vance and Schultz, 1993).

Vance and Li (1996) investigate the rotordynamic characteristics of a two-bladed, pocket gas damper seal by coastdown and rap (impact) tests. Impact experiments show the pocket gas damper seal to have an effective damping coefficient two orders of magnitude larger than a labyrinth seal of the same dimensions. Coastdown test results illustrate that the pocket damper seal significantly reduces rotor imbalance response. On the other hand, the measurements also reveal that the leakage rate of the pocket gas damper seal is about 30% larger than that of the labyrinth seal. Note that the test labyrinth seal has a see-through clearance equal to the inlet clearance (0.1016 mm) of the two-bladed, pocket gas damper seal, while the outlet clearance of the pocket damper seal is twice as large as its inlet clearance.

Li and Vance (1995) study experimentally the effects of clearance ratios and number of teeth on pocket gas damper seals on order to identify a design strategy for maximizing seal damping coefficients while decreasing seal leakage. Rap test results demonstrate that both the effective damping coefficient and the seal leakage decrease with a reduction in the clearance ratio and an increase in the number of teeth. At extreme conditions, test results show that the damping level of a two-bladed, pocket damper seal with a see-through clearance is comparable to that of a labyrinth seal of the same dimensions. These experiments further verify that the divergent clearance along the flow direction is a key feature of gas pocket damper seals to provide large positive damping coefficients.

Laos and Vance (1997) compare the rotordynamic performance of a four-bladed, pocket gas damper seal to a two-bladed, pocket gas damper seal by coastdown tests with a rough rotor surface. Both seals have the same diameter and axial length. The tests shows that the four-bladed pocket damper seal provides more equivalent damping than the two-bladed pocket damper seal for a rotating journal. Richards, et al. (1995) report

of successful applications of a four-bladed, four-pocket gas damper seals to eliminate subsynchronous vibration in back-to-back industrial compressors.

Systematic experiments to identify the force coefficients of a two-bladed, tooth-on-stator labyrinth seal with a diverging clearance and its modified version as a four-pocket gas damper seal have been conducted recently (Ransom, 1997). The seals are tested without rotation and at two journal speeds (1,500 and 3,000 rpm) and seal supply to ambient pressure ratios from 1 to 3. Calibrated impact loads excite a flexibly supported housing holding the test seal. A parameter identification procedure allows the determination of the seal dynamic force coefficients over a frequency range. The tests demonstrate the four-pocket, two-bladed gas damper seal to have a direct damping coefficient one order of magnitude larger than that of the labyrinth seal. In the test rig configuration, the damper seal is more stable dynamically though it provides a negative direct stiffness coefficient. For all test conditions, both seals show some small amount of cross-coupling effects which could not be discerned with accuracy since the measured cross-forces are well within the experimental uncertainty.

Theoretical models for the design and prediction of the pocket gas damper seal are yet insufficient when compared to the experimental investigations and successful industrial applications. Vance and Sundararajan (1993) develop a simple model for gas pocket damper seals based on the earlier theory for gas pocket damper actuators. The model only accounts for axial flow through the seal and neglects the effects of fluid viscosity, flow turbulence and the circumferential swirl flow resulted from rotor rotation and fluid pre-swirl. Although the model predicts both direct stiffness and damping coefficients with limited accuracy compared to experimental results, it can not provide values of the cross-coupled dynamic force coefficients. Neither the pocket pressure variation in the circumferential direction nor the flow across the gap between the radial baffle tip and the rotor surface are accounted for. However, prior experimental results at the Rotordynamic Laboratory show the geometric parameters of the radial baffle to have a significant influence on the dynamic force performance of the gas pocket damper seal. A comparison of the damping performance of a pocket gas damper seal with different

radial baffles is shown in Figure 2. When non uniform baffles with baffle tips lower than the seal tooth tips are installed in the seal cavity, these can not retard the circumferential flow effectively, and then the gas pocket damper seal looses most of its damping capability.

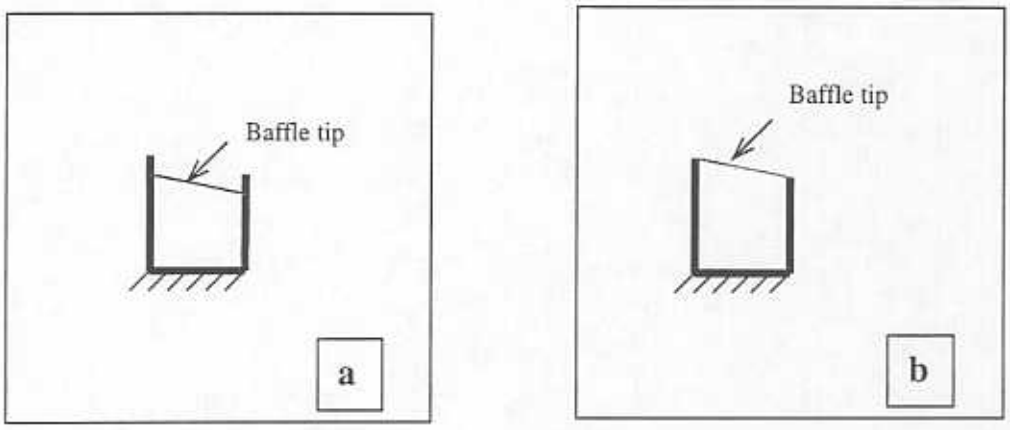

Figure 2. Pocket damper seal with slightly different partition baffle configurations.
(a) Baffle tips are lower than seal tooth tips, (b) Baffle tips are flush with seal tooth tips

A comparison of predictions versus measurements made by Li (1995) show that the *earlier* model (Vance and Sundararajan, 1993) overpredicts the seal damping coefficients. However, in other instance Vance and Schultz (1993) report the *earlier* model underpredicts the damping coefficient when the inlet pressures is above 4.0 bars. The two-bladed damper seal tested has a deeper cavity than the seal investigated by Li (1995).

A more complete flow model of multiple-tooth, multiple-pocket gas damper seals is needed to improve the prediction of leakage and dynamic force coefficients while still accounting for more practical operating conditions and desired design features in high performance turbomachinery.

2. BULK-FLOW MODEL FOR MULTIPLE-TOOTH, MULTIPLE-POCKET GAS DAMPER SEALS

The fluid flow in a multiple-tooth, multiple-pocket gas damper seal is generally fully turbulent due to the large axial pressure gradient across the seal, the high rotor surface speed and low fluid viscosity. The axial pressure drop in short length seals with a few teeth can be large enough to induce sonic flow conditions at the seal discharge plane.

Experimental measurements for pocket gas damper seals at the Turbomachinery Laboratory of Texas A&M University have shown that the temperature variation across the tested seals is less than 5% of the inlet fluid temperature. Additionally, Yang et al. (1994) demonstrate the effect of temperature variations to be negligible on typical gas seal dynamic forced performance. Hence, the fluid in the seal is regarded as an isothermal ideal gas with density $\rho = P/V_*^2$, where $V_* = \left(ZR_gT\right)^{1/2}$ is a characteristic velocity proportional to the fluid sonic speed and Z is the fluid compressibility factor. The pressure in each pocket region varies in the circumferential direction only since the grooves are typically deep and of short axial length.

Iwatsubo (1980) introduces a bulk-flow model to characterize the compressible flow in labyrinth cavities. The circumferential flow in the labyrinth seal is represented by a one-control-volume model and the axial momentum equation is replaced by an empirical leakage formula. Childs and Scharrer (1986b) improve Iwatsubo's one-control-volume bulk flow model by including the area rate of change in the circumferential direction neglected by Iwatsubo. Two control-volume bulk-flow models have also been developed to consider flow variations in seal cavities (Scharrer, 1988; Wyssmann, et. al., 1984). The calculation domain is divided into two control volumes, one in the seal cavity accounting for the vortex flow and another one for the jet flow between the cavity and strip tip.

Forte and Latini (1998) compare these bulk-flow models and point out no apparent advantages from the two-control-volume model over the one-control-volume model. Comparisons for selected experimental results show that the one-control-volume model predicts the direct damping coefficient better than the two-control-volume model. For labyrinth seals, the two-control-volume model appears to improve the prediction of the cross-coupled stiffness coefficients, which are mainly determined by the circumferential flow in seal cavities. However, the circumferential flow becomes of secondary importance in the multiple-pocket damper seals since the radial baffles effectively retard the development of the swirl flow in the gas pockets. Hence, a one-control-volume bulk-flow model is adopted in this research.

2.1 GOVERNING FLOW EQUATIONS AT THE SEAL POCKETS (CAVITIES)

A multiple-pocket damper cavity module is shown in Figure 3. The circumferential groove is divided into (N_c) identical pockets of angular extent $2\beta = 2\pi / N_c$. The bulk-flow field in the gas damper seal varies periodically in the circumferential direction. A one-control-volume bulk-flow model (see Figure 4) is applied to derive the governing equations at the i_{th} two-bladed cavity module. Following Childs (1993), the isothermal, viscous compressible bulk-flow in the gas pocket is characterized by the following continuity, circumferential momentum and axial mass flow rate equations:

Continuity Equation

$$\frac{1}{V_*^2}\left[\frac{\partial (PA)_i}{\partial t} + \frac{\partial (PAU)_i}{R_a \partial \Theta}\right] + \zeta_r (\dot{m}_{i+1} - \dot{m}_i) = 0 \tag{2}$$

Circumferential Momentum Equation

$$\frac{1}{V_*^2}\left[\frac{\partial (PAU)_i}{\partial t} + \frac{1}{R_a}\frac{\partial (PAU^2)_i}{\partial \Theta}\right] + \zeta_r (\dot{m}_{i+1} U_i - \dot{m}_i U_{i-1}) = -\frac{A_i}{R_a}\frac{\partial P_i}{\partial \Theta} + \Delta \tau_{xi} \tag{3}$$

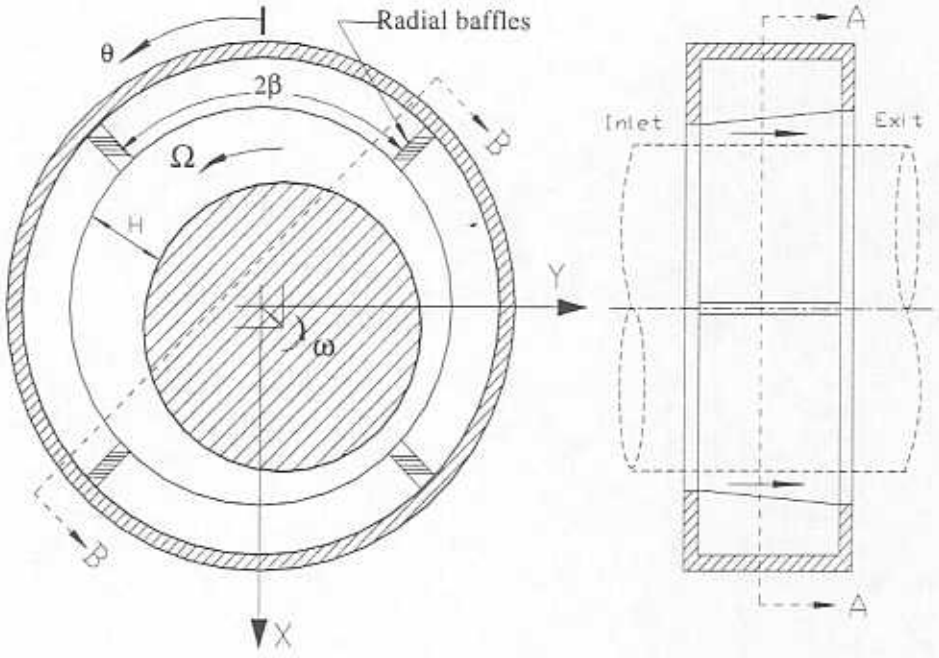

Section "A –A" Section "B – B"

Figure 3. A typical gas damper pocket cavity module.

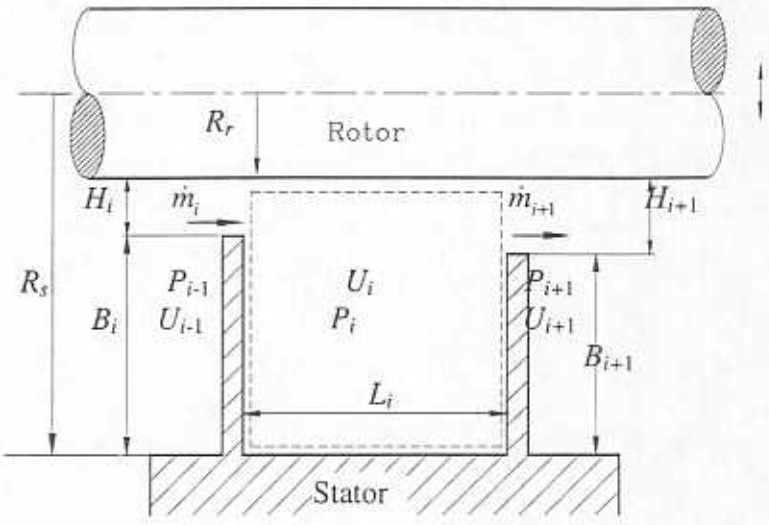

Figure 4. One control volume model for pocket gas damper seal.

Axial Mass flow Rate Equations

$$\dot{m}_i = \frac{(\mu_c \mu_f H)_i}{V_*^2}\sqrt{p_{i-1}^2 - P_i^2}$$
$$\dot{m}_{i+1} = \frac{(\mu_c \mu_f H)_{i+1}}{V_*^2}\sqrt{P_i^2 - b_c P_{i-1}^2} \qquad (4)$$

where $\dot{m}_i$, $\dot{m}_{i+1}$ are the axial mass flow ratios per unit circumferential length across the upstream and downstream teeth of the i_{th} axial cavity. P_i and U_i are the bulk-flow pressure and circumferential velocity in the i_{th} cavity, respectively. A_i is the cross-section area of the axial cavity, and $b_c = 1.0$ for unchoked flow while $b_c = 0.0$ for choked flow. The coefficient $\zeta_r = R_r / R_a$ accounts for the effect of the pocket depth when the differential control-volume is calculated with R_a, the average radius of the TOS seal. The last term on the RHS of the momentum equation is the shear stress difference $\Delta\tau_{xi}$, which combines the contributions of the shear stresses on both seal stator and rotor surfaces.

2.2 Shear Stress Model

Hirs bulk-flow theory (Hirs, 1973) and Moody's friction formulae have been successfully used for the dynamic analysis of turbulent flows in liquid seals and gas seals (San Andrés, 1991, Yang, et. al., 1994). In thin film flows, the shear stress difference $\Delta\tau_{xi}$ combines the contributions of the shear stresses acting on both seal stator and rotor surfaces (Launder and Leschziner, 1978), i.e.,

$$\Delta\tau_{xi} = -\frac{\mu L_i}{D_{hi}}\left[k_{xi}U_i - k_{fi}\frac{\Omega R_r}{2}\right] \qquad (5)$$

where D_{hi} is the seal hydraulic diameter typically defined as $\{2L_i(B_i + H_i)/(L_i + B_i + H_i)\}$ for the i_{th} two-bladed cavity module. The shear stress parameters k_{xi} and k_{fi} are expressed as:

$$k_{fi} = \zeta_r k_{ri}; \qquad k_{si} = \frac{\zeta_r k_{ri}}{2} + \frac{(\zeta_s L_i + B_i + B_{i+1})}{2L_i} k_{si} \tag{6}$$

where $\zeta_r = R_r / R_a$ and $\zeta_s = R_s / R_a$ are the ratios of the rotor radius and the seal outer radius to the average radius of the seal. k_{ri} and k_{si}, the rotor and stator turbulent shear stress parameters, are functions of the local Reynolds numbers and the Moody's friction factors at the stator and rotor surfaces, i.e.,

$$k_{ri} = f_{ri} Re_{ri}; \qquad k_{si} = f_{si} Re_{si} \tag{7}$$

where,

$$Re_{ri} = \left[\frac{\rho D_{hi}}{\mu} \sqrt{(U_i - \Omega R_r)^2 + W_i^2} \right]$$

$$Re_{si} = \left[\frac{\rho D_{hi}}{\mu} \sqrt{U_i^2 + W_i^2} \right] \tag{8}$$

and,

$$f_{ri} = 0.00137 \left[1 + \frac{10^4 e_r}{(B_i + H_i)} + \frac{10^6}{\mathrm{Re}_{ri}} \right]^{0.333}$$

$$f_{si} = 0.00137 \left[1 + \frac{10^4 e_s}{(B_i + H_i)} + \frac{10^6}{\mathrm{Re}_{si}} \right]^{0.333} \tag{9}$$

2. 3 EQUATIONS FOR THE CIRCUMFERENTIAL FLOW ACROSS THE RADIAL BAFFLE TIPS

The radial baffle (partition wall), depicted in Figure 5, acts as a flow resistance in the circumferential direction. A local pressure difference occurs across the radial baffle between two adjacent pockets. Here, the fluid accelerates through the thin gap between the baffle and the rotor surface from the upstream pocket to the downstream pocket. The thickness of the baffle is (S) and the gap between the baffle tip and rotor surface is (H_w). The upstream and downstream pressures across the baffle are referred as P_{uw} and P_{dw}, respectively. The pressure and circumferential velocity of the bulk-flow across the baffle

tip are noted as P_w and U_w.

Since the thickness of the baffle is relatively small, it is assumed that the circumferential bulk-flow velocity U_w over the baffle tip is uniform. Direct application of the circumferential momentum equation (3) to the control volume at the baffle tip yields,

$$\frac{1}{V_*^2}\frac{\partial (PAU)_i}{\partial t} + \zeta_r(\dot{m}_{i+1}U_i - \dot{m}_i U_{i-1}) = -\frac{A_i}{R_a}\frac{\partial P_i}{\partial \Theta} + \Delta\tau_{xi} \tag{10}$$

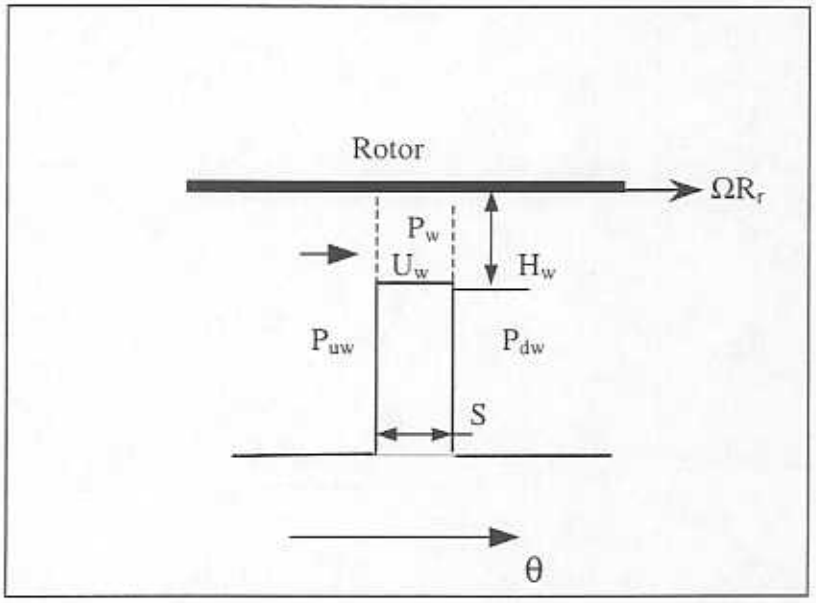

Figure 5. A schematic view of the (partition) radial baffle

where $A_i = L_i H_{wi}$. For a small baffle thickness (S), the circumferential pressure gradient is approximately expressed as:

$$\frac{A_i}{R_a}\frac{\partial P_i}{\partial \Theta} \equiv \frac{L_i H_{wi}\left(P_{dwi} - P_{uwi}\right)}{S_i} \tag{11}$$

Substituting equation (11) and shear stress expression (5) into equation (10) gives,

$$\frac{1}{V_*^2}\frac{\partial (PAU)_i}{\partial t} + \zeta_r(\dot{m}_{i+1}U_i - \dot{m}_i U_{i-1}) = -\frac{L_i H_{wi}}{S_i}(P_{dwi} - P_{uwi}) - \frac{\mu L_i}{D_{hwi}}\left[k_{xi}U_i - k_{fi}\frac{\Omega R_r}{2}\right] \tag{12}$$

Note that U_i is referred as U_{wi} at the radial baffle. Rearranging the equation above yields the following relation for the circumferential bulk-flow velocity at the radial baffle:

$$U_{wi} = \alpha_{ri}\left(\frac{\Omega R_r}{2}\right) + \alpha_{si}U_{i-1} + \alpha_{wi}\left(\frac{D_{hw}(P_{uw} - P_{dw})}{\mu}\right)_i + \alpha_{ti}\frac{\partial (PAU)_{wi}}{\partial t} \tag{13}$$

where D_{hw} is the seal hydraulic diameter at the baffle defined as $\{2LH_w/(L+H_w)\}$. The coefficients α_{ri}, α_{si}, α_{wi} and α_{ti} in the equation above are expressed as:

$$\alpha_{ri} = \frac{k_{fi}}{k_{xi} + (\zeta_r \dot{m}_b D_{hw}/\mu L)_i}; \qquad \alpha_{si} = \frac{(\zeta_r \dot{m}_s D_{hw}/\mu L)_i}{k_{xi} + (\zeta_r \dot{m}_b D_{hw}/\mu L)_i}$$

$$\alpha_{wi} = \frac{H_{wi}/S_i}{k_{xi} + (\zeta_r \dot{m}_b D_{hw}/\mu L)_i}; \qquad \alpha_{ti} = -\frac{(D_{hw}/\mu L)_i}{k_{xi} + (\zeta_r \dot{m}_b D_{hw}/\mu L)_i}\left(\frac{1}{V_*^2}\right) \tag{14}$$

Note that the circumferential bulk-flow velocity at the baffle consists of three components due to the rotor surface speed, the local upstream pre-swirl and the local flow acceleration due to the pressure difference across the baffle. The coefficients α_{ri}, α_{si}, α_{wi} and α_{ti} above depend on seal geometric parameters and operating conditions. Without radial baffles in the seal axial cavities equation (13) reduces to a circumferential momentum equation for a centered labyrinth seal since the pressure difference term on the RHS of the equation disappears.

The baffle pressure P_{wi} needs to be specified for the closure of the flow conditions at the radial baffle. Constantinescu and Galetuse (1975) study the inertial pressure drop across

a step region (see Figure 6). The viscous stresses are negligible in the step area when compared to the abrupt change in momentum. From their investigation, the relation between the pressure difference (ΔP) and sliding velocity (V) can be approximately expressed as:

$$\Delta P = P_1 - P_2 = \frac{1}{2}\xi_w \rho V^2 \tag{15}$$

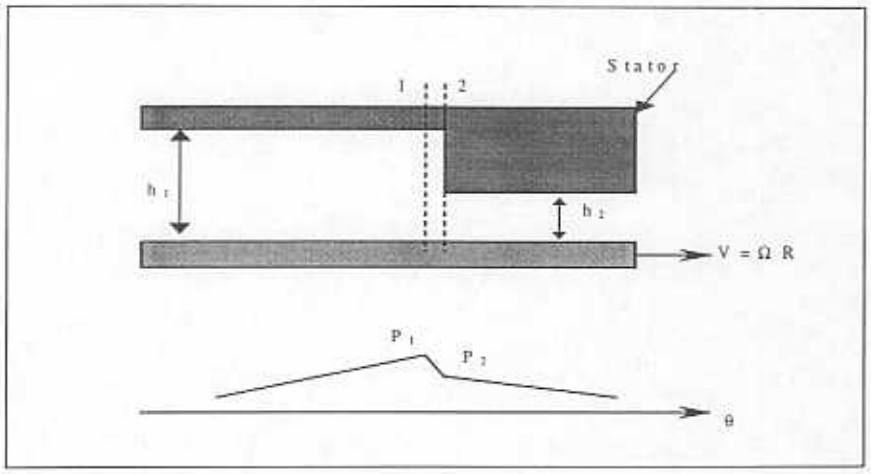

Figure 6. Conceptual description of pressure drop at a step region due to inertial effects.

For turbulent flow, the value of the loss factor ξ_w ranges from 0.0 to 0.2 when the thickness ratio (h_1/h_2) is larger than 5. Hence, an expression of pressure P_{wi} at the baffle is obtained by applying equation (15) to the radial baffle region as:

$$P_{wi} = P_{uw}\left[1 - \frac{1}{2}\frac{\xi_w (\Omega R_r)^2}{V_*^2}\right] \tag{16}$$

2.4 Flow Governing Equations in Dimensionless Form

A set of dimensionless variables is defined as,

$$\overline{U} = U/V_* ; \qquad \overline{P} = P/P_* ; \qquad \overline{L} = L/L_* ; \qquad \overline{H} = H/L_* ;$$

$$\overline{W} = W/V_* ; \qquad \overline{\mu} = \mu/\mu_* ; \qquad \overline{D}_h = D_h/L_* ; \qquad \overline{B} = B/L_* ;$$
$$\overline{R}_a = R_a/R_r ; \qquad \overline{A} = A/L_*^2 ; \qquad \overline{e} = e/L_* ; \tag{17}$$
$$\tau = \omega t ; \qquad \overline{\dot{m}} = \left(\frac{V_*}{L_* P_*}\right)\dot{m}$$

where P_*, μ_* and L_* are a set of characteristic variables equal to supply pressure, fluid viscosity and the height of the first seal tooth, respectively.

In dimensionless form, the bulk-flow governing equations (2-4) can be expressed as:

Continuity Equation

$$\sigma \frac{\partial(\overline{PA})_i}{\partial \tau} + \frac{\partial(\overline{PA}\,\overline{U})_i}{\overline{R}_a \partial \Theta} + \zeta(\overline{\dot{m}}_{i+1} - \overline{\dot{m}}_i) = 0 \tag{18}$$

Circumferential Momentum Equation

$$\mathrm{Re}_t \frac{\partial(\overline{PA}\,\overline{U})_i}{\partial \tau} + \mathrm{Re}_c \frac{\partial(\overline{PA}\,\overline{U}^2)_i}{\overline{R}_a \partial \Theta} + \mathrm{Re}_c \zeta(\overline{\dot{m}}_{i+1}\overline{U}_i - \overline{\dot{m}}_i \overline{U}_{i-1})$$
$$= -\mathrm{Re}_c \frac{\overline{A}_i}{\overline{R}_a}\frac{\partial \overline{P}_i}{\partial \Theta} - \frac{\overline{\mu}\overline{L}_i}{\overline{D}_{hi}}\left[k_{xi}\overline{U}_i - k_{Ji}\frac{\Lambda}{2}\right] \tag{19}$$

Axial Mass flow Rate Equations

$$\overline{\dot{m}}_i = (\mu_c \mu_f \overline{H})_i \sqrt{\overline{P}_{i-1}^2 - \overline{P}_i^2}$$
$$\overline{\dot{m}}_{i+1} = (\mu_c \mu_f \overline{H})_{i+1} \sqrt{\overline{P}_i^2 - b_c \overline{P}_{i-1}^2} \tag{20}$$

with the following flow parameters,

$$\Lambda = \frac{\Omega R_r}{V_*} ; \qquad \sigma = \frac{\omega R_r}{V_*} ; \qquad \zeta = \zeta_r\left(\frac{R_r}{L_*}\right) = \left(\frac{R_r}{R_a}\right)\left(\frac{R_r}{L_*}\right)$$
$$\mathrm{Re}_p = \frac{\rho_* V_* L_*}{\mu_*} = \frac{P_* L_*}{\mu_* V_*} ; \qquad \mathrm{Re}_c = \left(\frac{L_*}{R_r}\right)\mathrm{Re}_p \tag{21}$$
$$\mathrm{Re}_t = \sigma\left(\frac{L_*}{R_r}\right)\mathrm{Re}_p = \sigma\,\mathrm{Re}_c$$

where Λ and σ are the rotor surface speed and whirl frequency parameters, respectively. ζ is a geometric factor related to the aspect ratio of the cavity. Re_p is a reference pressure flow Reynolds number, and Re_c is an advection flow Reynolds number denoting the ratio of fluid advection forces to viscous flow forces. Re_t is a typical squeeze film Reynolds number which represents the importance of the squeeze film flow relative to the pressure flow and the shear flow components. Correspondingly, the following expressions are derived:

$$\begin{aligned} \overline{\rho} &= \overline{P} \ ; \\ \mathrm{Re}_r &= \mathrm{Re}_p \left[\frac{\overline{\rho}\overline{D}_h}{\overline{\mu}} \sqrt{(\overline{U} - \Lambda)^2 + \overline{W}^2} \right] ; \\ \mathrm{Re}_s &= \mathrm{Re}_p \left[\frac{\overline{\rho}\overline{D}_h}{\overline{\mu}} \sqrt{\overline{U}^2 + \overline{W}^2} \right] \end{aligned} \tag{22}$$

2.5 DIMENSIONLESS FLOW EQUATIONS AT THE RADIAL BAFFLE

In dimensionless form, the flow equations at the radial baffles are expressed as:

$$\overline{U}_{wi} = \alpha_{ri}\left(\frac{\Lambda}{2}\right) + \alpha_{si}\overline{U}_{i-1} + \mathrm{Re}_p\,\alpha_{wi}\left(\frac{\overline{D}_{hw}(\overline{P}_{uw} - \overline{P}_{dw})}{\overline{\mu}}\right)_i + \mathrm{Re}_t\,\alpha_{ti}\frac{\partial(\overline{PA}\,\overline{U})_{wi}}{\partial\tau} \tag{23}$$

$$\overline{P}_{wi} = \overline{P}_{uwi}\left[1.0 - \frac{1}{2}\xi_w\Lambda^2\right] \tag{24}$$

where

$$\alpha_{ri} = \frac{k_{fi}}{k_{xi} + \mathrm{Re}_p\left(\zeta_r\overline{m}_b\overline{D}_{hw}/\overline{\mu}\overline{L}\right)_i} ; \qquad \alpha_{si} = \frac{\mathrm{Re}_p\left(\zeta_r\overline{m}_s\overline{D}_{hw}/\overline{\mu}\overline{L}\right)_i}{k_{xi} + \mathrm{Re}_p\left(\zeta_r\overline{m}_b\overline{D}_{hw}/\overline{\mu}\overline{L}\right)_i}$$

$$\alpha_{wi} = \frac{\overline{H}_{wi}/\overline{S}_i}{k_{xi} + \mathrm{Re}_p\left(\zeta_r\overline{m}_b\overline{D}_{hw}/\overline{\mu}\overline{L}\right)_i} ; \qquad \alpha_{ti} = -\frac{\left(\overline{D}_{hw}/\overline{\mu}\overline{L}\right)_i}{k_{xi} + \mathrm{Re}_p\left(\zeta_r\overline{m}_b\overline{D}_{hw}/\overline{\mu}\overline{L}\right)_i} \tag{25}$$

2.6 PERTURBATION ANALYSIS

A perturbation analysis of the flow field within the seal renders the required zeroth-order and first-order equations for determination of the seal leakage and dynamic forces coefficients. Let the rotor center whirl at frequency (ω) with small amplitude motions (e_X, e_Y) about the seal concentric position. In general, the seal clearance is represented by the following equations:

$$\overline{H} = \overline{H}_0 + \varepsilon_j H_j e^{i\tau}; \quad i = \sqrt{-1}; \quad j = X, Y$$
$$H_X = \cos\theta; \quad H_Y = \sin\theta \tag{26}$$

where ($\varepsilon_j = e_j / L_c$) is a dimensionless small rotor displacement parameter, and the subscripts "j" (= X, Y) denote the directions of rotor motion. For small amplitude rotor motions, all flow variables can be expressed as the superposition of steady-state and first-order dynamic fields. In general,

$$\Phi = \Phi_0 + \varepsilon_j \Phi_j e^{i\tau}, \quad \Phi = \overline{U}, \overline{P}, k_x, k_j, \mathrm{Re}_r, \mathrm{Re}_z, ..., etc. \tag{27}$$

Substitution of equations (26-27) into the governing equations yields the zeroth and first-order equations describing the equilibrium flow field and the (harmonic) perturbed flow field, respectively. These equations are:

- Zeroth-order equations at the i_{th} seal cavity

For convenience, the subscript "0" is omitted for all zeroth-order variables.

Continuity Equation

$$\frac{\partial(\overline{PA}\,\overline{U})_i}{\overline{R}_u \partial\Theta} + \zeta(\dot{\overline{m}}_{i+1} - \dot{\overline{m}}_i) = 0 \tag{28}$$

Circumferential Momentum Equation

$$\mathrm{Re}_c \frac{\partial(\overline{PA}\,\overline{U}^2)_i}{\overline{R}_a \partial\Theta} + \mathrm{Re}_c\,\zeta(\overline{\dot{m}}_{i+1}\overline{U}_i - \overline{\dot{m}}_i\overline{U}_{i-1}) = -\mathrm{Re}_c \frac{\overline{A}_i}{\overline{R}_a}\frac{\partial \overline{P}_i}{\partial\Theta} - \frac{\overline{\mu}\overline{L}_r}{\overline{D}_{hi}}\left[k_{xi}\overline{U}_i - k_{fi}\frac{\Lambda}{2}\right] \tag{29}$$

The zeroth-order axial mass flow ratio equations have the same form as equation (20).

- Zeroth-order equations at the seal radial baffle

For convenience, the subscript "0" is omitted for all zeroth-order variables.

$$\overline{U}_{wi} = \alpha_{ri}\left(\frac{\Lambda}{2}\right) + \alpha_{si}\overline{U}_{i-1} + \mathrm{Re}_p\,\alpha_{wi}\left(\frac{\overline{D}_{hw}(\overline{P}_{uw} - \overline{P}_{dw})}{\overline{\mu}}\right)_i \tag{30}$$

$$\overline{P}_{wi} = \overline{P}_{uwi}\left[1.0 - \frac{1}{2}\xi_w\Lambda^2\right] \tag{31}$$

- First-order equations at the i_{th} seal cavity (pocket)

For convenience, the subscript "0" is omitted for all zeroth-order variables.

Continuity Equation

$$\mathrm{i}\sigma\left(\overline{PL}H_j + \overline{A}\overline{P}_j\right)_i + \frac{1}{\overline{R}_a}\frac{\dot{o}}{\partial\Theta}\left(\overline{PA}\,\overline{U}_j + \overline{P}\,\overline{UL}H_j + \overline{UA}\overline{P}_j\right)_i + \eta_{mhi}H_j + \eta_{mpi}\left(\overline{P}_j\right)_i + \eta_{mpui}\left(\overline{P}_j\right)_{i-1} + \eta_{mpdi}\left(\overline{P}_j\right)_{i+1} = 0 \tag{32}$$

Circumferential Momentum Equation

$$\mathrm{i}\,\mathrm{Re}_t\left(\overline{PA}\,\overline{U}_j + \overline{P}\,\overline{UL}H_j + \overline{UA}\overline{P}_j\right)_i + \frac{\mathrm{Re}_c}{\overline{R}_a}\frac{\dot{o}}{\partial\Theta}\left(2\overline{P}\,\overline{UA}\,\overline{U}_j + \overline{P}\,\overline{U}^2\overline{L}H_j + \overline{U}^2\overline{A}\overline{P}_j\right)_i$$

$$\mathrm{Re}_c\left(\eta_{uu}\overline{U}_j + \eta_{uh}H_j + \eta_{up}\overline{P}_j\right)_i + \mathrm{Re}_c\left[-\eta_{uui}\left(\overline{U}_j\right)_i + \eta_{upui}\left(\overline{P}_j\right)_{i-1} + \eta_{updi}\left(\overline{P}_j\right)_{i+1}\right] \tag{33}$$

$$= -\frac{\mathrm{Re}_c}{\overline{R}_a}\left(\overline{A}\frac{\partial\overline{P}_j}{\partial\Theta} + \overline{L}\frac{\partial\overline{P}}{\partial\Theta}H_j\right)_i + \left(\eta_{xu}\overline{U}_j + \eta_{xh}H_j + \eta_{xp}\overline{P}_j\right)_i + \eta_{xpui}\left(\overline{P}_j\right)_{i-1}$$

Axial Mass Flow Rate Equations

$$\left(\overline{\dot{m}}_j\right)_i = \eta_{hi} H_j + \eta_{pdi}\left(\overline{P}_j\right)_i + \eta_{pui}\left(\overline{P}_j\right)_{i-1}$$

$$\left(\overline{\dot{m}}_j\right)_{i+1} = \eta_{hi+1} H_j + \eta_{pdi+1}\left(\overline{P}_j\right)_{i+1} + \eta_{pui+1}\left(\overline{P}_j\right)_i \tag{34}$$

where the subscripts "j" (= X, Y) denote the directions of rotor motion. The η coefficients arising from the perturbation of the empirical axial leakage terms and turbulent shear stress terms are given in *Appendix A*.

- First-order equations at the radial baffle

Similarly, a perturbation analysis on the flow across the radial baffle between adjacent pockets is performed. The first-order velocity and pressure at the partition baffle are expressed as:

$$\left(\overline{P}_j\right)_{wi} = \left(\beta_{jpu}\overline{P}_{uwj} + \beta_{jpd}\overline{P}_{dwj}\right)_i$$

$$\left(\overline{U}_j\right)_{wi} = \frac{1}{\left(1-\alpha_{jursw}\right)_i}\left(\alpha_{jh}H_j + \alpha_{jpu}\overline{P}_{uwj} + \alpha_{jpd}\overline{P}_{dwj}\right)_i \qquad j = X,Y \tag{35}$$

where the β_j and α_j coefficients, given in *Appendix A*, arise from the first-order perturbation of the boundary conditions at the partition baffle.

2.7 Boundary Conditions

Uniform supply pressure (P_s) and back pressure (P_b) are specified at the inlet and exit planes of the seal as determined by the operation conditions. A uniform inlet pre-swirl ratio is adopted as well. The assumption precludes the case of a perturbation of the circumferential flow upstream of the seal inlet plane.

In a centered gas damper seal with several identical circumferential cavities (pockets), the zeroth-order solution for just one pocket is needed since, by circumferential symmetry, the other pockets have identical steady-state pressure and mean circumferential velocity

fields. Therefore, the pressure and velocity at the partition baffles should be specified as boundary conditions when calculating the flow flied in a two-bladed damper cavity module.

- If the i_{th} two-bladed cavity module is an interior module ($1 < i < N_w$), its upstream boundary conditions P_{i-1} and U_{i-1} are obtained directly from the preceding iterative calculation. The following upstream boundary conditions are only used for the first cavity module ($i = 1$):

$$(P_0)_{i-1} = P_s; \quad (U_0)_{i-1} = \alpha\Omega R_r$$
$$(P_j)_{i-1} = 0; \quad (U_j)_{i-1} = 0 \tag{36}$$

- For the i_{th} two-bladed cavity module ($1 < i < N_w$), the downstream boundary P_{i+1} is also obtained directly from the preceding iterative calculation. If the cavity module is the last one ($i = N_w$), the downstream pressure is equal to

$$(P_0)_{i+1} = P_b; \qquad (P_j)_{i+1} = 0 \tag{37}$$

- In the circumferential direction, if the i_{th} two-bladed cavity is a pocket cavity module, equations (30), (31) and (35) are used as boundary conditions for the zeroth-order and first-order flow fields, respectively. On the other hand, periodicity boundary conditions are adopted for a labyrinth cavity module, i.e.,

$$U_0(6) = U_0(6 + 2\pi); \qquad U_j(6) = U_j(6 + 2\pi)$$
$$P_0(\theta) = P_0(\theta + 2\pi); \qquad P_j(\theta) = P_j(\theta + 2\pi) \tag{38}$$

2.8 Evaluation of Seal Rotordynamic Force Coefficients

The zeroth-order solution determines the steady-state pressure and circumferential velocity fields. The total seal leakage ($\dot{M}$) is evaluated with the following formula:

$$\dot{M} = R_r \sum_{n=1}^{N_c} \int_{-\beta}^{+\beta} \dot{m}_i d\theta \tag{39}$$

The first-order solution leads to the determination of the seal dynamic force (stiffness and damping) coefficients by integration of the complex first-order pressure field (P_j) over the rotor surface (Lund, 1987),

$$(K_{ij} + \mathrm{i}\omega C_{ij}) = -\sum_{k=1}^{Nw} \left[LR_r \sum_{n=1}^{N_c} \int_{-\beta}^{+\beta} P_j^n H_i \, d\theta \right]_k \quad i, j = X, Y; \quad \mathrm{i} = \sqrt{-1} \tag{40}$$

For the concentric seal position, $K_{YY} = K_{XX}$, $K_{YX} = -K_{XY}$, $C_{YY} = C_{XX}$, and $C_{YX} = -C_{XY}$. Furthermore, for gas pocket damper and labyrinth seals the force coefficients given by equation (40) are functions of the excitation frequency since the fluid is compressible.

In summary, a one-control-volume bulk-flow model is developed to determine the leakage and rotordynamic force coefficients of multiple-teeth, multiple-pocket gas damper seals. Governing equations for the fluid flow within the seal cavity and across the radial baffles are derived. Flow turbulence and viscosity are accounted for in the model through shear stress parameters based on Moody's formulae. The effects of fluid compressibility and excitation frequency on the seal dynamic force characteristics are also included.

3. NUMERICAL METHOD OF SOLUTION

3.1 NUMERICAL SOLUTION OF THE ZEROTH-ORDER EQUATIONS

A control-volume finite difference scheme is implemented to solve the coupled, nonlinear PDEs of mass and momentum transport. The flow field is represented by a series of discrete nodal pressures and circumferential velocities on staggered grids (Patankar, 1980). The velocity nodes are located at points which lie at interfaces midway between the nodes where the pressure is determined as shown in Figure 7. An advantage of the staggered grid is that the potential, unrealistic wavy pressure solutions arising from a single grid are avoided. Zeroth-order discrete algebraic difference equations are derived by integrating the governing equations on finite size control volumes and using the SIMPLEC algorithm of Van Doormaal and Raithby (1984). The discrete difference equations for circumerential momentum and pressure correction are given in *Appendix B*. The effectiveness of this approach has been demonstrated in the turbulent flow analysis for fluid film bearings and seals (San Andrés, 1991, Yang et al., 1993). An upwinding scheme is used for the advection terms in order to make the algorithm more stable.

The difference governing equations are solved numerically in an iterative procedure. The empirical leakage equation (Childs, 1993) is used to guess an initial pressure field within the seal. The velocity components are first calculated from the circumferential momentum equation using the guessed pressure field, and then a pressure correction equation based on the continuity equation provides corrected pressure and velocity fields. The updated pressure and velocity fields are substituted into the momentum and pressure correction equations again resulting in (generally) more accurate velocity and pressure field solutions. A line-by-line solution scheme is implemented to accelerate convergence of the algebraic solution. The iterative procedure above is repeated until the maximum difference between two consecutive iterations for the pressure field is less than 1×10^{-6} of the seal supply pressure. Also the ratio of the global mass flow residuals to the total mass flow across the seal is used to

monitor the convergence of the numerical scheme. Typically, the ratio of the residual mass flow to the seal total mass flow is required to be below a prescribed tolerance value (about 1×10^{-6}).

The computer for calculation of the leakage and dynamic force coefficients for multiple-pocket gas damper seals has been completed. The numerical solution procedure to solve for zeroth-order solutions is summarized in the flow chart shown in Figure 8. For a centered pocket gas damper seal, the radial baffles (partition walls) divide a cavity into several identical pockets, and then the steady-state bulk-flow field in the gas damper seal varies periodically along the circumferential direction. Hence, the zeroth-order difference equations are solved only for one gas pocket in each axial cavity.

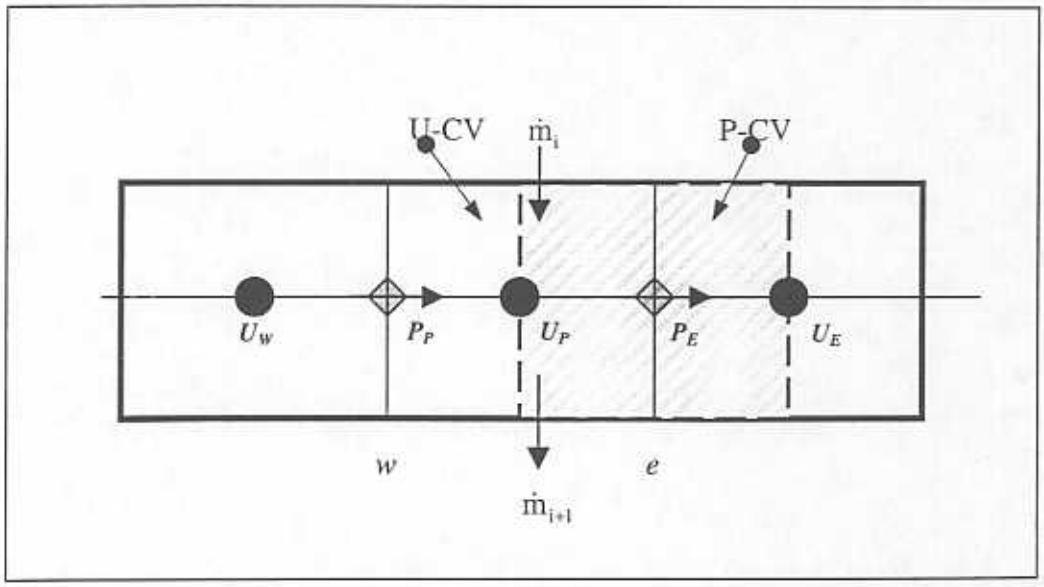

Figure 7. Diagram of staggered grids and finite control volumes.

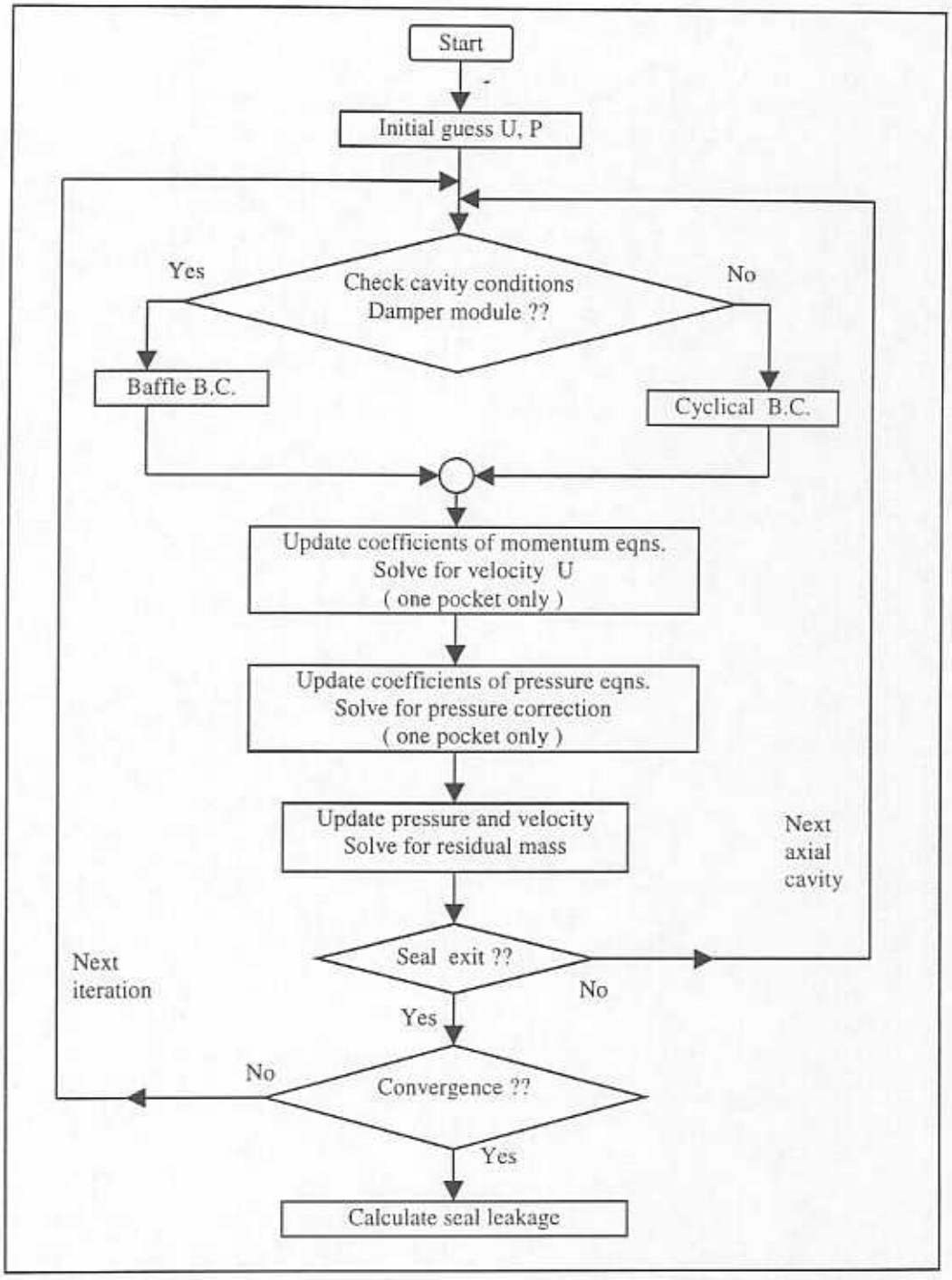

Figure 8. Flow chart for zeroth-order numerical solution

3.2 NUMERICAL SOLUTION OF THE FIRST-ORDER EQUATIONS

The discrete difference equations for the first-order circumerential momentum and pressure correction are given in *Appendix C*. The numerical solution procedure for the zeroth-order difference equations is also suitable for the first-order equations. The coefficients in the first-order discrete difference equations are fully determined by the zeroth-order solution. However, the first-order solution of the flow in an axial cavity (between two blades) is no longer a periodic function of the circumferential coordinate (Θ). Therefore, the first-order difference equations should be solved on all gas pockets within a module. Figure 9 shows the flow chart to calculate the flow first-order solution and the seal rotordynamic force coefficients.

3.3 CLOSURE

A finite difference scheme based on the SIMPLEC semi-implicit approach is implemented to solve both the zeroth and first order governing equations. The zeroth-order solution determines the steady-state cavity pressure and circumferential velocity as well as the seal axial leakage. The first-order solution leads to the determination of the dynamic force characteristics in the gas damper seal. The dynamic forces of the seal are calculated from the integration of the complex first-order pressure field over the journal surface. Typically, less than 3% difference in the magnitudes of dynamic force coefficients is detected when comparing the results from a circumferential 10-node grid to those from a 20-node grid on each pocket for two-bladed, four-pocket gas damper seals. Therefore, the computer program appears to be insensitive to the variations of computational mesh.

The validation of the bulk-flow model and the computational algorithm are demonstrated next by comparing the numerical predictions with existing experimental results for gas damper seals.

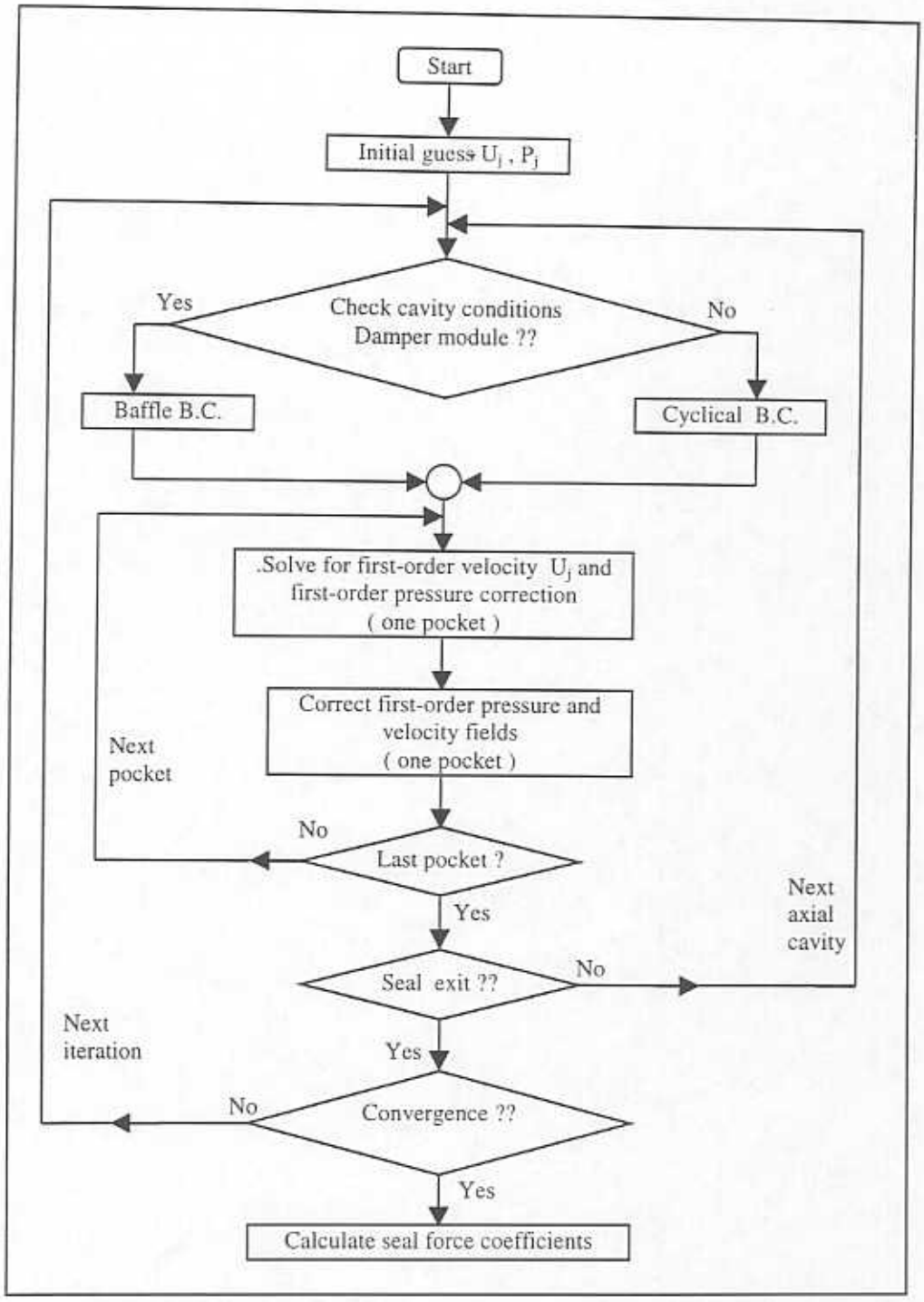

Figure 9. Flow chart for first-order numerical solution

4. VALIDATION OF BULK-FLOW MODEL TO EXPERIMENTAL MEASUREMENTS

This section presents computational predictions for the leakage and rotordynamic force coefficients of multiple-pocket gas damper seals. The predictions from the bulk-flow model are compared to the numerical results of the earlier model (Vance and Sundararajan, 1993) and experimental data from two multiple-pocket gas damper seals tested at the Rotordynamics Laboratory. The validity of the bulk-flow model is confirmed through these comparisons.

4.1 COMPARISONS TO TEST RESULTS FROM A FOUR-POCKET GAS DAMPER SEAL

A systematic experimental research program is conducted at TAMU Rotordynamics Laboratory to identify the rotordynamic force coefficients of multiple-pocket gas damper seals. Ransom (1997) describes a test apparatus for identification of the stiffness and damping coefficients of gas seals from their forced response due to impact loads. Experiments are conducted at increasing journal speeds and increasing inlet pressures. Calibrated impact guns excite in two orthogonal directions a flexibly supported housing holding the test seal. A frequency domain parameter identification procedure allows the determination of the seal dynamic force coefficients over a frequency range. Ransom (1997) also reports the uncertainty analysis for the identified dynamic force coefficients. The largest uncertainties in the test stiffness and damping coefficients are 6 kN/m and 3 N sec/m, respectively. The mass flow rate has an uncertainty as large as 0.6 g/sec. Each experiment is conducted twice at given operating conditions. The repeatability of the measured dynamic force coefficients is not as good as expected, thus all test results are shown in the following comparisons with numerical predictions from the present bulk-flow model.

The tested seal is a two-blade, four-pocket gas damper seal. The seal nominal dimensions and test conditions are listed in Table 1. The experiments are carried out at null rotor speed and two rotational speeds (1.5 and 3.0 krpm). No effort is made to induce inlet pre-swirl to the flow. The maximum seal supply to ambient pressure ratio is

limited to 2.0 since the pocket gas damper seal generates a large negative direct stiffness which overcomes the support structure stiffness and causes the seal to suck against the journal at larger pressure ratios. In the tests, the (impact induced) seal dynamic forced responses show a decaying vibratory motion with a natural frequency ranging from 39 to 49 Hz. Thus, the computed results are obtained for an average rotor excitation frequency of 44 Hz.

Table 1. Two-blade, four-pocket damper seal nominal dimensions and test conditions (Ransom, 1997)

No. of circumferential pockets, N_c = 4
No. of seal axial cavities, N_w = 1
Rotor radius, R_r = 2.500" (63.500 mm)
Seal outer radius, R_s = 2.770" (70.358 mm)
Seal inside pitch length, L = 1.374" (34.900 mm)
Seal inlet clearance, H_s = 0.005" (0.127 mm)
Seal inlet tooth height, B_s = 0.265" (6.731 mm)
Seal exit clearance, H_b = 0.010" (0.254 mm)
Seal exit tooth height, B_b = 0.60" (6.604 mm)
Radial baffle clearance, H_w = 0.0075" (0.1905 mm)
Radial baffle thickness, S = 0.0984" (2.500 mm)
Inlet air temperature, T = 73 °F (296 °K)
Gas constant, R_g = 639.31 in-lb/lbm-°R (287 J/kg-K)
Air specific heat ratio, γ = 1.4
Seal inlet pressure, P_s = 22 ~ 29.4 psia (1.5195 ~ 2.023 bar)
Seal discharge pressure, P_b = 14.7 psia (1.013 bar)
Rotor rotation speed, 0.0, 1500, 3000 rpm
Excitation frequency for predictions, 44 Hz
Seal inlet pre-swirl ratio, α = 0.0

- Comparison of seal mass flow rates

Both test and computed results show that rotor speed has negligible influence on the seal mass flow rate (leakage). The (null rotor speed) mass flow rate vs. pressure ratio is depicted in Figure 10. The comparison shows that the bulk-flow model slightly overpredicts the seal leakage (4% ~ 10%) for the two pressure ratios tested. Clearly, the discrepancy between the test results and predictions increases as the pressure ratio increases. The bulk-flow model predicts seal leakage better as compared to the *earlier* model of Vance and Sundararajan (1993).

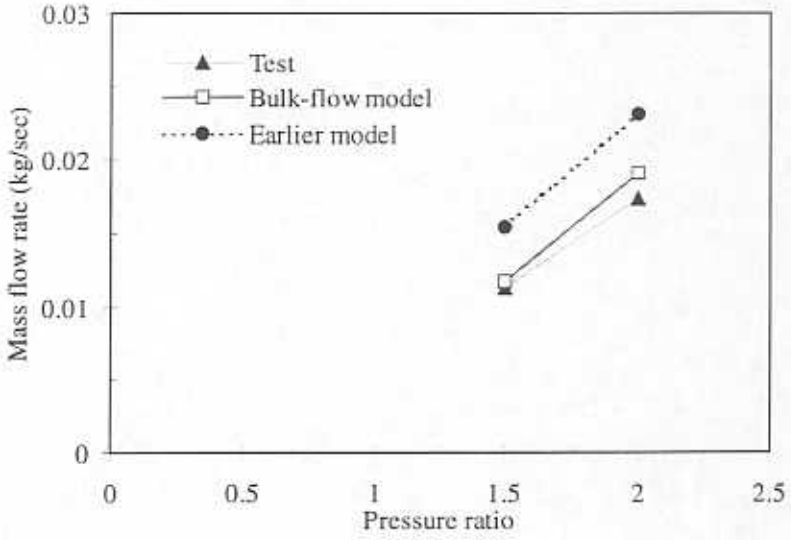

Figure 10. Comparison of leakage mass flow rates for a two-blade, four-pocket gas damper seal (Ransom, 1997). (P_b = 1.013 bar, Ω = 0.0 rpm)

- Comparisons of direct force coefficients

Figure 11 illustrates the seal direct force coefficients (stiffness and damping) from both models[1] and test results vs. pressure ratio for a rotor speed equal to 3,000 rpm. In general, both computational models overpredict the seal damping coefficient. At a

[1] These refer to the current bulk-flow model and the one of Vance and Sundararajan (1993) hereafter referred as the *earlier* model.

pressure ratio of 2.0, the present model overpredicts the damping coefficients (59% ~ 67%) while the earlier model largely overpredicts the damping coefficients (465% ~ 490%). The bulk-flow model underpredicts the magnitude of the seal stiffness coefficients (10% ~ 50%) while the earlier model overpredicts the magnitude of the seal stiffness coefficients (200% ~ 430%) in the tested pressure range. Note that the values of the test seal (negative) direct stiffness are rather small.

- Direct stiffness

Figures 12 and 13 show comparisons of predicted ($K_{XX} = K_{YY}$) and experimental direct stiffness coefficients (K_{XX} and K_{YY}) versus rotor speed for test pressure ratios equal to 1.5 and 2.0. The model correctly predicts negative direct stiffness coefficients and of magnitude increasing as the pressure ratio increases. The experimental results show stiffness of different magnitude thus revealing a degree of orthotropy in the test apparatus. The test K_{XX} appears as a weak function of rotor speed while the theoretical stiffness is insensitive to this variable parameter. Overall, the current model underpredicts the magnitude of the direct stiffness coefficient for most test conditions. At a pressure ratio equal to 2.0, the bulk-flow model underpredicts the measured K_{XX} (20% ~ 35%) and K_{YY} (30% ~ 40%).

- Direct damping

Comparisons of predictions and test direct damping coefficients (C_{XX} , C_{YY}) for the two-blade, four-pocket gas damper seal are shown in Figures 14 and 15, respectively. The test results show asymmetric direct damping coefficients, which may have been caused by a slightly off centered seal. The model correctly predicts the direct damping coefficients to be positive and to increase with increasing pressure ratios. Both predicted and test results demonstrate the direct damping coefficients (C_{XX} , C_{YY}) to be insensitive to rotor speed, with the exception of the test C_{YY} which has a sharp upturn at a rotor speed of 1,500 rpm and at pressure ratio equal to 2.0. In the pressure range tested,

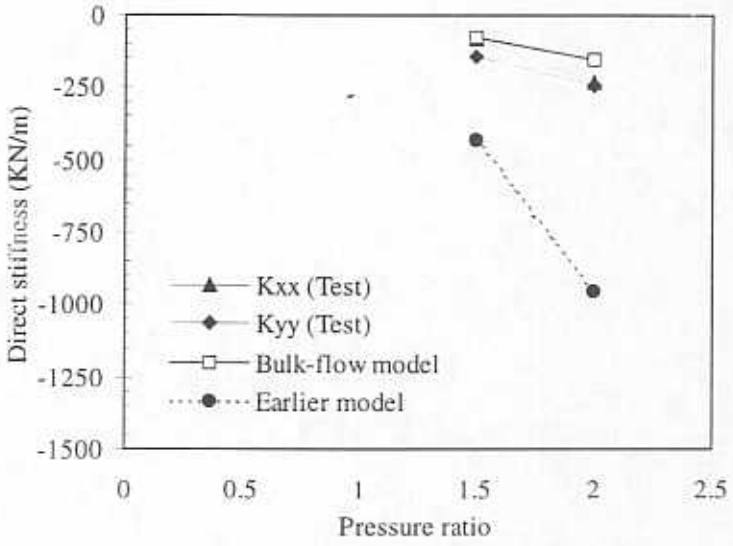

(a) Direct stiffness

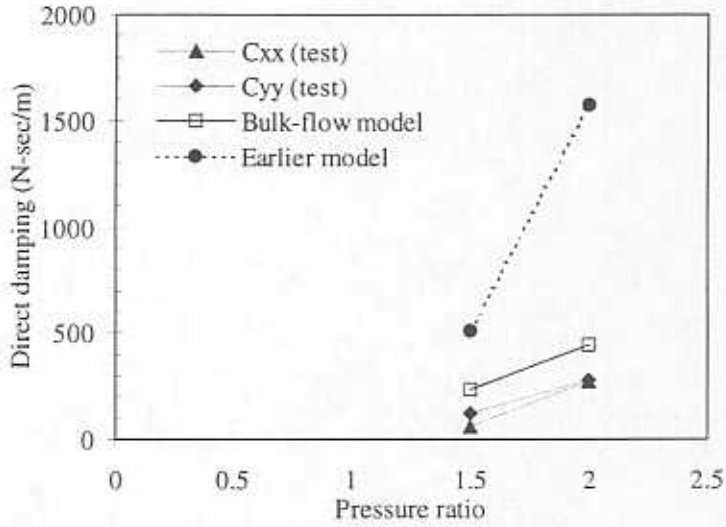

(b) Direct damping

Figure 11. Comparison of seal force coefficients for a two-blade, four-pocket gas damper seal (Ransom, 1997).
(P_b = 1.013 bar, Ω = 3,000 rpm)
(a) Direct stiffness; (b) Direct damping

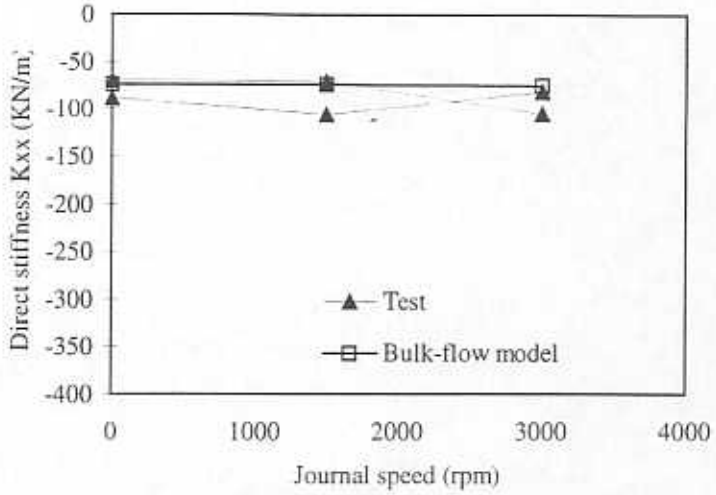

(a) Pressure ratio = 1.5

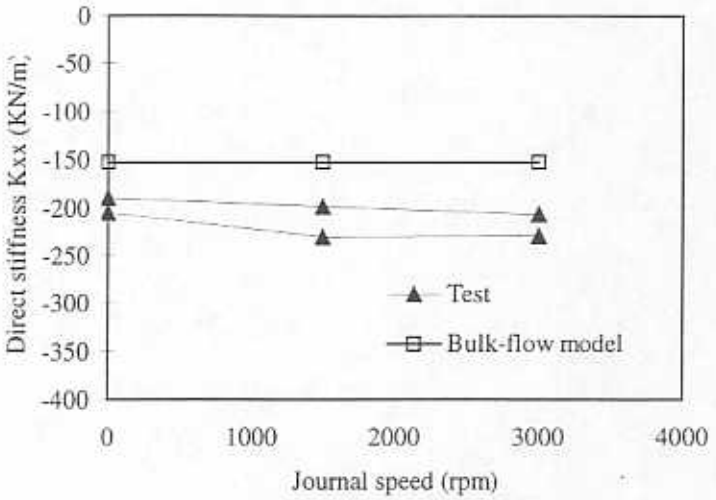

(b) Pressure ratio = 2.0

Figure 12. Direct stiffness (K_{xx}) vs. rotor speed for a two-blade, four-pocket gas damper seal (Ransom, 1997).
(P_b = 1.013 bar)
(a) Pressure ratio = 1.5; (b) Pressure ratio = 2.0

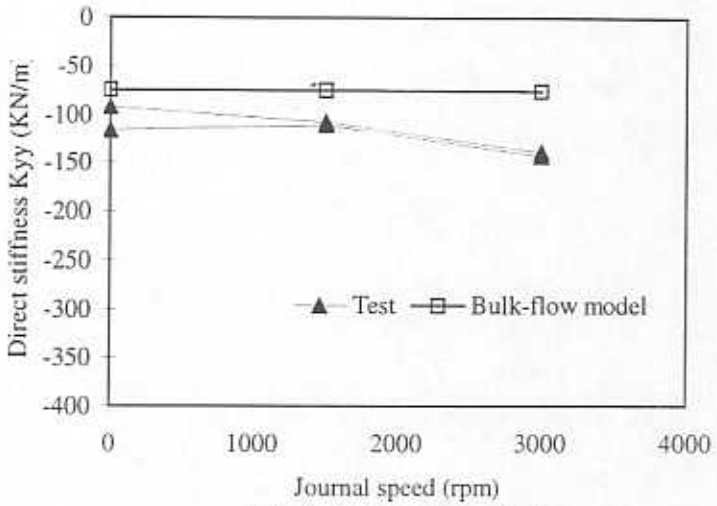

(a) Pressure ratio = 1.5

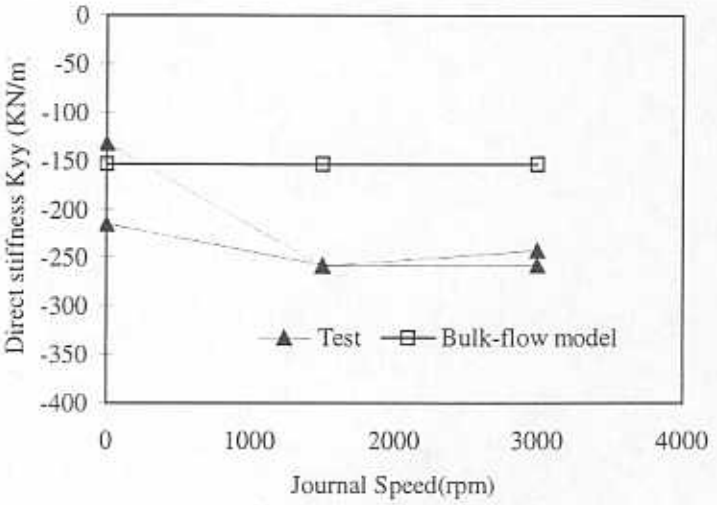

(b) Pressure ratio = 2.0

Figure 13. Direct stiffness (K_{yy}) vs. rotor speed for a two-bladed, four-pocket gas damper seal (Ransom, 1997).
(P_b = 1.013 bar)
(a) Pressure ratio = 1.5; (b) Pressure ratio = 2.0

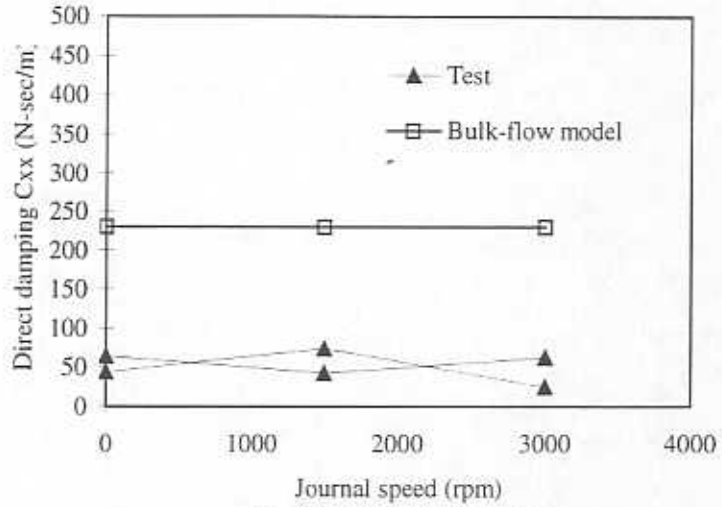

(a) Pressure ratio = 1.5

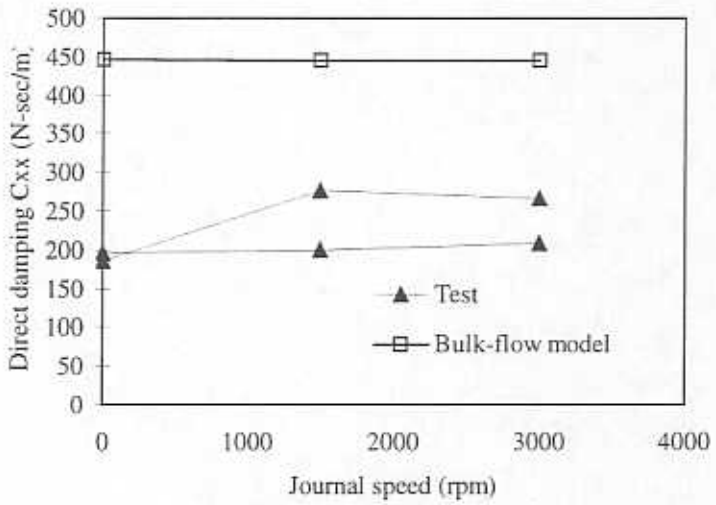

(b) Pressure ratio = 2.0

Figure 14. Direct damping (C_{xx}) vs. rotor speed for a two-blade, four-pocket gas damper seal (Ransom, 1997).
(P_b = 1.013 bar)
(a) Pressure ratio = 1.5; (b) Pressure ratio = 2.0

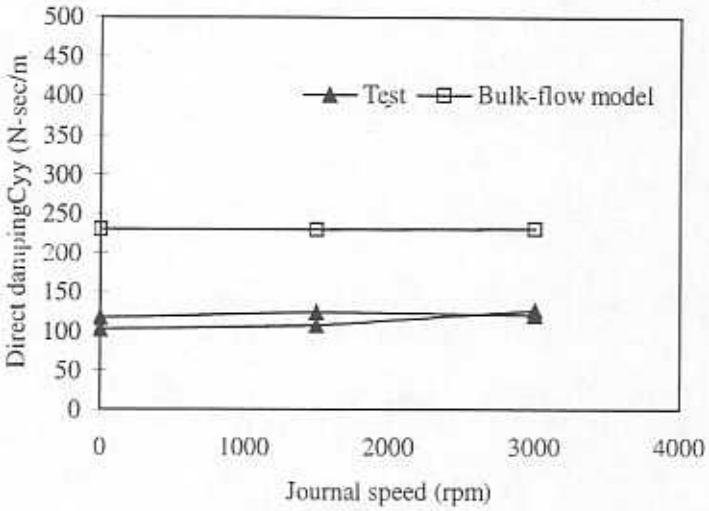

(a) Pressure ratio = 1.5

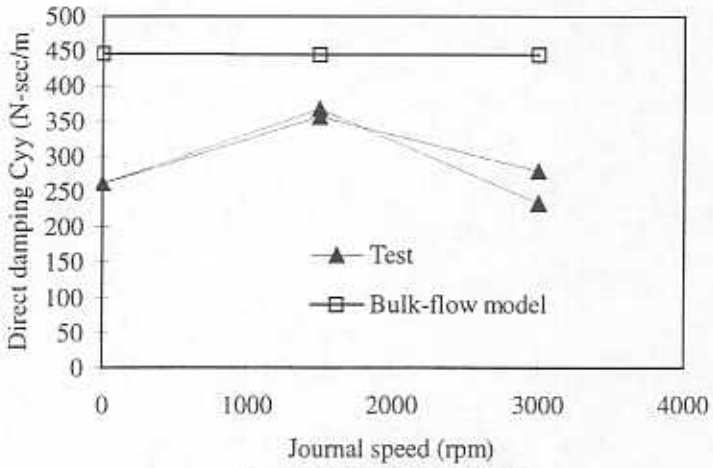

(b) Pressure ratio = 2.0

Figure 15. Direct damping (C_{yy}) vs. rotor speed for a two-blade, four-pocket gas damper seal (Ransom, 1997).
(P_b = 1.013 bar)
(a) Pressure ratio = 1.5; (b) Pressure ratio = 2.0

the model overpredicts C_{XX} (70% ~ 420%) and overpredicts C_{YY} (60% ~ 125%). The predictions agree better with the measured damping coefficients at the high pressure condition since the relative error (uncertainty) decreases as the pressure ratio increases.

- Cross-coupled stiffness

Figure 16 shows the bulk-flow model to predict well the cross-coupled stiffness coefficient K_{XY}, except for the unusual test results at a speed of 1,500 rpm. For instance, a zero cross-coupled stiffness is expected at null journal speed whereas the test results show a non-zero identified K_{XY} for a pressure ratio of 2.0. The model reasonably predicts the magnitudes of the cross-coupled stiffness coefficients to increase slightly with increasing rotor speed since the radial baffles effectively block the circumferential flow in the seal cavity. However, no apparent trends are observed from the measured cross-coupled stiffness coefficients versus rotor speed.

The bulk-flow model fails to predict the identified K_{YX} (see Figure 17) because the experimental results do not show the asymmetric relation, $K_{XY} = -K_{YX}$, to hold for the test conditions. However, accounting for the experimental uncertainty ± 6 KN/m, both bulk-flow model and experimental results verify that the pocket gas damper seal has very small cross-coupled force coefficients.

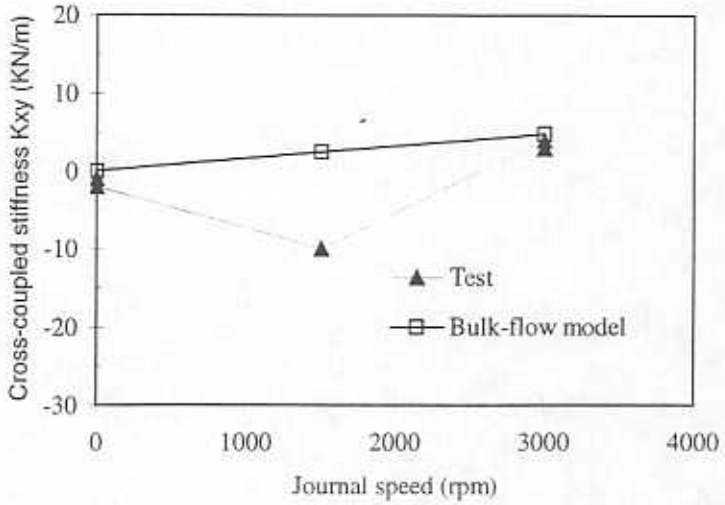

(a) Pressure ratio = 1.5

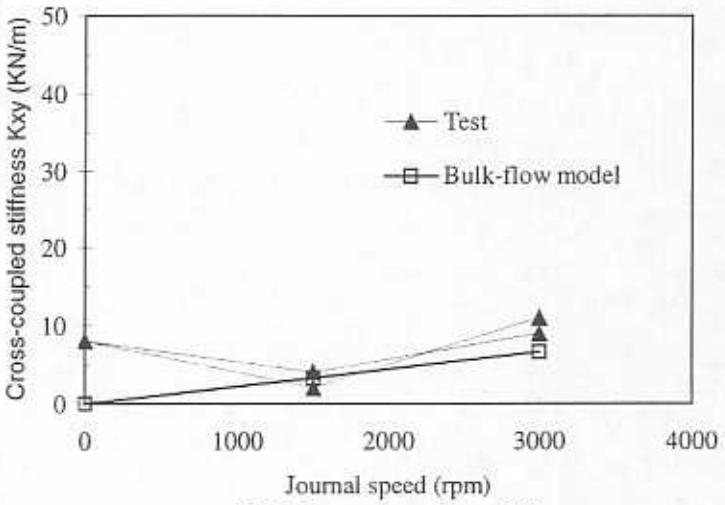

(b) Pressure ratio = 2.0

Figure 16. Cross-coupled stiffness (K_{xy}) vs. rotor speed for a two-blade, four-pocket gas damper seal (Ransom, 1997).
(P_b = 1.013 bar)
(a) Pressure ratio = 1.5; (b) Pressure ratio = 2.0

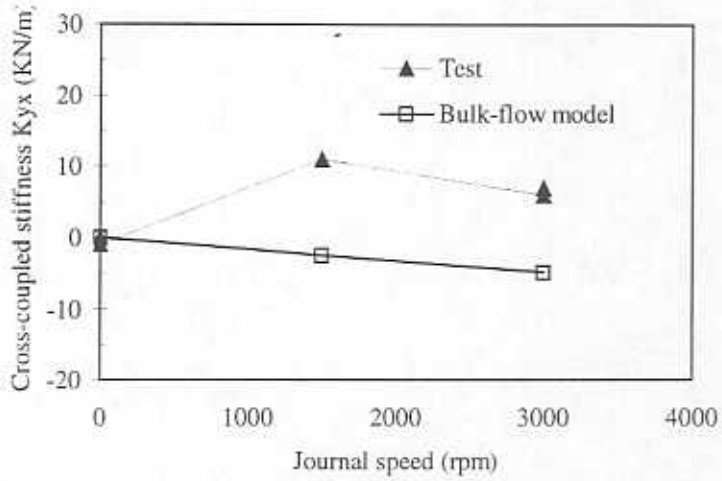

(a) Pressure ratio = 1.5

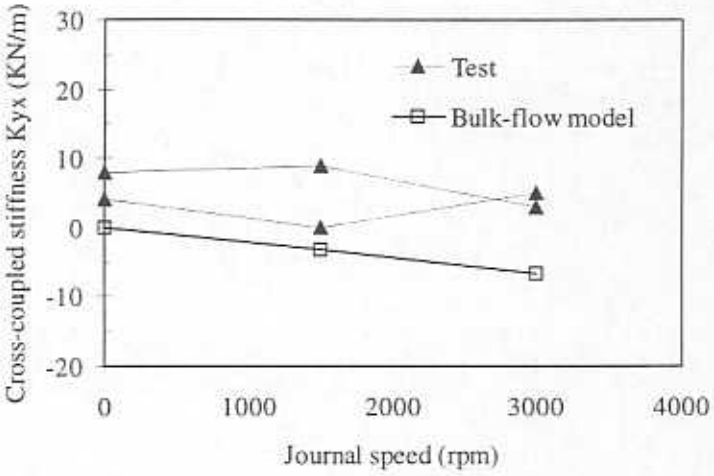

(b) Pressure ratio = 2.0

Figure 17. Cross-coupled stiffness (K_{yx}) vs. rotor speed for a two-blade, four-pocket gas damper seal (Ransom, 1997).
(P_b = 1.013 bar)
(a) Pressure ratio = 1.5; (b) Pressure ratio = 2.0

4.2 Comparisons to test results from a four-blade, four-pocket gas damper seal

Aguilar (1998) performs experiments to measure the leakage and identification of force coefficients from a four-blade, four-pocket gas damper seal on the same vertical test rig used by Ransom (1997). The seal nominal dimensions and test conditions are given in Table 2. The test seal consists of two four-pocket cavity modules separated by one labyrinth cavity module. The pocket cavities are twice as long as the labyrinth cavity length. In each four-pocket cavity, the ratio of inlet clearance to exit clearance is 0.5. The damper cavities of this seal are shorter and deeper than those from the two-blade damper seal tested by Ransom (1997). Experiments are performed at null rotor speed and four rotational speeds (1.5, 3.0, 4.5 and 6.0 krpm). No effort is made to induce inlet pre-swirl to the flow. The maximum seal supply to ambient pressure ratio is limited to 2.5. In the tests, the (impact induced) seal dynamic forced responses show a decaying vibratory motion with a natural frequency ranging from 36 to 42 Hz. Thus, the bulk-flow predictions are calculate for an average rotor excitation frequency of 39 Hz.

- Comparison of seal mass flow rates

As in the prior seal studied, rotor speed has a negligible influence on the seal (leakage) mass flow rate. Figure 18 depicts the seal mass flow rate vs. pressure ratio at a rotor speed of 3,000 rpm. The comparison of predicted and tests results shows that the discrepancy between the experimental values and the bulk-flow model predictions increases slightly as the pressure ratio increases. At the pressure ratio equal to 2.5, the bulk-flow model overpredicts the seal leakage 3% while the *earlier* model overpredicts the seal leakage by as much as 9%.

Table 2. four-blade, four-pocket damper seal nominal dimensions and test conditions (Aguilar, 1998)

No. of circumferential pockets, N_c = 4
No. of seal axial cavities, N_w = 3
Rotor radius, R_r = 2.500" (63.500 mm)
Seal outer radius, R_s = 2.9250" (74.295 mm)
Damper cavity length = 0.500" (12.700 mm)
Damper cavity inlet clearance, H_a = 0.005" (0.127 mm)
Damper cavity inlet tooth height, B_a = 0.420" (10.668 mm)
Damper cavity exit clearance, H_b = 0.010" (0.254 mm)
Damper cavity exit tooth height, B_b = 0.415" (10.541 mm)
Labyrinth cavity length = 0.250" (6.350 mm)
Radial baffle clearance, H_w = 0.0075" (0.1905 mm)
Radial baffle thickness, S = 0.0787" (2.000 mm)
Inlet air temperature, T = 73 °F (295 °K)
Gas constant, R_g = 639.31 in-lb/lbm-°R (287 J/kg-K)
Air specific heat ratio, γ = 1.4
Seal inlet pressure, P_s = 22 ~ 36.75 psia (1.5195 ~ 2.5325 bar)
Seal discharge pressure, P_b = 14.7 psia (1.013 bar)
Rotor rotation speed, 0.0, 1500, 3000, 4500, 6000 rpm
Excitation frequency for predictions = 39 Hz
Seal inlet pre-swirl ratio, α = 0.0

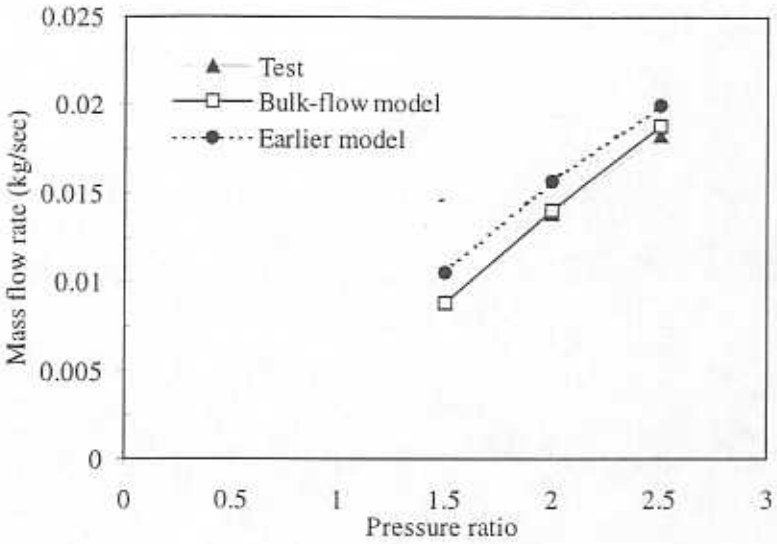

Figure 18. Comparison of mass flow rates for a four-bladed, four-pocket gas damper seal (Aguilar, 1998). (P_b = 1.013 bar, Ω = 3,000 rpm)

- Comparisons of direct force coefficients

The measured and predicted direct force coefficients (stiffness and damping) for the four-blade, four-pocket gas damper seal are shown in Figure 19 at a rotor speed of 3,000 rpm. Typically, both computational models, bulk flow and *earlier*, overpredict the seal direct stiffness coefficient. At a pressure ratio of 2.5, the bulk-flow model overpredicts the magnitude of the seal stiffness coefficients (10% ~ 66%) while the earlier model overpredicts the magnitude of the seal stiffness coefficients (220% ~ 380%). In the test pressure range, the bulk-flow model improves the prediction of the seal damping coefficient significantly. The comparison show that the bulk-flow model underpredicts (C_{XX}) 8% and overpredicts (C_{YY}) 16% at a pressure ratio of 2.5. The *earlier* model largely overpredicts the damping coefficients (205% ~ 285%).

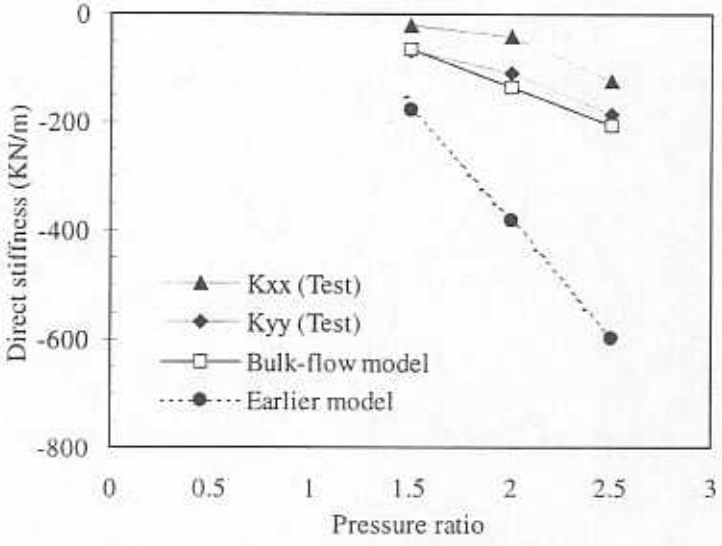

(a) Direct stiffness

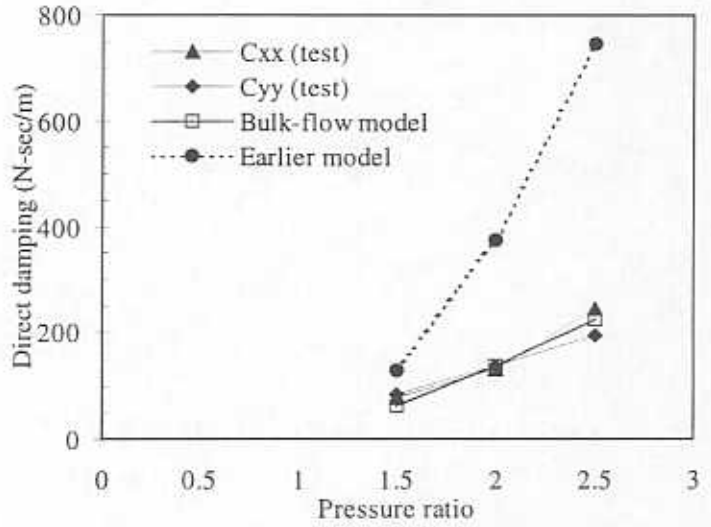

(b) Direct damping

Figure 19. Comparison of seal force coefficients for a four-bladed, four-pocket gas damper seal (Aguilar, 1998).
(P_b = 1.013 bar, Ω = 3,000 rpm)
(a) Direct stiffness coefficients; (b) Direct damping coefficients

5. CONCLUSIONS

Laboratory experiments and turbomachinery applications have demonstrated that multiple-pocket gas damper seals offer enough (direct) damping to effectively eliminate subsynchronous vibration and to reduce the amplitude of rotor imbalance response while passing through critical speeds. The needs to achieve efficient high speed, oil-free turbomachinery give importance to the development of reliable gas damper seals able to replace oil-lubricated squeeze film dampers. This requirement is also mandated by stringent environmental constraints.

A one control-volume, bulk-flow model for the prediction of leakage, pressure field and rotordynamic force coefficients of multiple-teeth, multiple-pocket gas damper seals is completed. A *CFD* algorithm is implemented to solve for the nonlinear partial differential equations governing the bulk-flow in the arcuate pockets of a gas damper seal. The computational model accounts for the effects of fluid viscosity, flow turbulence, and circumferential swirl flow on the seal dynamic force performance. The influence of the radial baffles on the circumferential flow in the seal pockets is considered with a sound physical model. Zeroth- and first-order bulk-flow equations describe the steady flow for a centered seal and with small amplitude rotor motions about the equilibrium position. Seal leakage and dynamic force coefficients are obtained from solutions to the zeroth and first-order equations, respectively.

The Fortran computer program developed calculates the leakage and dynamic force coefficients of multiple-teeth, multiple pocket gas damper seal as function of the seal geometry, rotor speed, pressure drop and excitation frequency. Computed predictions for leakage, damping and stiffness force coefficients are compared to experimental measurements from two multiple-pocket damper seals with diverging clearance. The test force coefficients are obtained from transfer functions of seal displacement versus (exciting) impact loads in two orthogonal directions. A frequency domain method with noise minimization is used for identification of the seal dynamic force coefficients.

Predictions and test results show that the seal leakage and direct force coefficients are insensitive to rotor speed, and whose magnitudes increase with increasing inlet to

discharge pressure ratios. Correlation of test and calculated mass flow rate is excellent for both seals. The model correctly predicts negative direct stiffness and large positive direct damping coefficients, as the experimental values evidence. For the two-blade, four pocket gas damper seal, the bulk-flow model underpredicts the direct stiffness coefficient and overpredicts the direct damping coefficient for all test conditions. For the four-blade, four-pocket gas damper seal, the agreement between the model predictions and the test direct force coefficients is very reasonable.

The predictions and test results show the cross-coupled stiffness coefficients to be small compared to the seal direct force coefficients under most experimental conditions. The radial baffles separating the arcuate pockets are very effective to reduce the development of the circumferential mean flow velocity. Predictions show the cross-coupled stiffness to increase slightly with increasing rotor speeds, while no distinct trend is obtained from the experimental results.

Further analysis and computational developments as well as systematic experiments are planned to include brush-seals at the discharge plane of gas pocket damper seals. This hybrid seal configuration is expected to provide more direct damping than for the seals tested to date.

ACKNOWLEDGEMENTS

The support of the State of Texas Advanced Technology Program and the Texas A&M Turbomachinery Consortium is gratefully acknowledged.

REFERENCES

Aguilar, R, 1998, "Test Results for a Four Blade, Four Pocket Gas Damper Seal," Preliminary Report, Rotordynamics Laboratory, Texas A&M University, May.

Alford, J. S., 1965, "Protecting Turbomachinery From Self-Excited Rotor Whirl," *ASME Journal of Engineering for Power*, pp. 333-344.

Benckert, H., and J. Wachter, 1980, "Flow Induced Spring Coefficients of Labyrinth Seals For Application in Rotordynamics," NASA CP 2133, pp. 189-212.

Childs, D. W., 1993, "Turbomachinery Rotordynamics: Phenomena, Modeling, & Analysis," John Wiley & Sons, Inc., New York, pp. 300.

Childs, D. W., and Kleynhans, G., 1993, "Theory versus Experiment for Short (L/D=1/6) Honeycomb and Smooth Annular Pressure Seals," Proceedings of the 14th ASME Vibration and Noise Conference, September 19-22, Albuquerque, New Mexico, pp. 173-179.

Childs, D. W. and Ramsey, C., (1991), "Seal-Rotordynamic Coefficient Test Results for a Model SSME ATD-HPFTP Turbine Interstage Seal with and Without a Swirl Brake", ASME Journal of Tribology, Vol. 113, pp. 198-203.

Childs, D. W., and Scharrer, J. K., 1986a, "Experimental Rotordynamic Coefficient Results for Teeth-on Rotor and Teeth-on-Stator Labyrinth Gas Seals", Journal of Engineering for Gas Turbines and Power, Vol. 108, pp. 599-604.

Childs, D. W., and Scharrer, J. K., 1986b, "An Iwatsubo-Based Solution for Labyrinth Seals: Comparison to Experimental Results", Journal of Engineering for Gas Turbines and Power, Vol. 108, pp. 325-331.

Childs, D. W., and Scharrer, J. K., 1988, "Theory Versus Experiment for the Rotordynamic Coefficient of Labyrinth Gas Seals: Part II - A Comparison to Experiment", Journal of Vibration, Acoustic, Stress, and Reliability in Design, Vol. 110, pp.281-287.

Childs, D. W., and Vance, J. M., 1997, "Annular Seals And the Rotordynamics of Compressors and Turbines," Proceedings of the 26th Turbomachinery Symposium, September 14-18, Houston, Texas, pp. 201-220.

Childs, D. W., Elrod, D., and Hals, K., 1989, "Annular Honeycomb Seals: Test Results for Leakage and Rotordynamic Coefficients; Comparisons to Labyrinth and Smooth Configurations," *ASME Journal of Tribology*, Vol. 111, pp. 293-301.

Constantinescu, V. N., and Galetuse, S., 1975, "Pressure Drop Due to Inertia Forces in Step Bearings," *ASME* Paper 75-Lub-34.

Doyle, H., 1980, "Field Experience with Rotordynamic Instability in High-Performance Turbomachinery," NASA CP 2133, *Proceedings of Workshop on Rotordynamic Instability Problems in High Performance Turbomachinery*, Texas A&M University, pp. 3-14.

Forte, P., and Latini, F., 1998, "Theoretical Rotordynamic Coefficients of Labyrinth Gas Seals: A Parameter Study on A Bulk Model," *Proceedings of the ISROMAC-7*, International Symposium on Transport Phenomena and Dynamics of Rotating Machinery, February, Honolulu, Hawaii, pp. 861-870.

Fozi, A. A., 1986, "An Examination of Gas Compressor Stability and Rotating Stall," Proceeding of a workshop on Rotordynamic Instability Problems in High-Performance Turbomachinery, Texas A&M University, NASA # 2443, pp. 19-33.

Gelin, A., Pugnet, J. M., Bolusset, D., and Friez, P., 1996, "Experience in Full Load Testing Natural Gas Centrifugal Compressors for Rotordynamics Improvements," ASME Paper # 96-GT-378.

Greathead, S., and Bostow, P., 1976, "Investigations into Load Dependent Vibrations of the High Pressure Rotor on Large Turbo-Generators," *Proceedings of the 1st International*

Conference on Vibrations in Rotating Machinery (ImechE), Cambridge, England, pp. 279-286.

Hawkins, L. Childs, D. W., and Hale Keith, 1989, "Experimental Results for Labyrinth Gas Seals with Honeycomb Stator: Comparisons to smooth-Stator and Theoretical Predictions", ASME Journal of Tribology, Vol. 111, No. 1, pp.161-168.

Iwatsubo, T., 1980, Evaluation of Instability Forces of Labyrinth Seals in Turbines or Compressors, Proceedings of a Workshop on Rotordynamic Instability Problems in High-Performance Turbomachinery at Texas A&M University, NASA 2133, pp. 139-167.

Kanki, H., Katayama, K., Morii, S., Mouri, Y., Umemura, S., Ozawa, U. and Oda, T., 1988, "High Stability Design for New Centrifugal Compressor," Proceeding of a workshop on Rotordynamic Instability Problems in High-Performance Turbomachinery, Texas A&M University, NASA # 3026, pp. 445-459.

Kwanka, K., 1997, "Rotordynamic Impact of Swirl Brakes on Labyrinth Seals with Smooth or Honeycomb Stators," ASME Paper 97-GT-232.

Laos, H., and Vance, J. M., 1997, "Rotordynamic Effects of Damper Seals," TRC-Seal-8-97, Turbomachinery Laboratory Research Progress Report, Texas A&M University, College Station, April.

Laundar, B. E., and Leschziner, M., 1978, "Flow in Finite-Width, Thrust Bearings Including Inertial Effects, I - Laminar Flow, II - Turbulent Flow," *ASME Journal of Lubrication Technology*, Vol. 100, pp. 330-345.

Li, J., 1995, "The Effect of A New Damper Seal on Rotordynamics," Master's Thesis, Texas A&M University, August.

Li, J., and Vance, J. M., 1995, "Effects of Clearance and Clearance Ratio on Two and Three Bladed TAMSEALs," TRC-Seal-4-95, Turbomachinery Laboratory Research Progress Report, Texas A&M University, College Station, April.

Lund, J. W., 1974, "Stability and Damped Critical Speeds of a Flexible Rotor in Fluid Film Bearings," ASME Journal of Engineering for Industry, Vol. 96, pp. 509-517.

Murphy, B. T., and Vance, J. M., 1980, "Labyrinth Seal Effects on Rotor Whirl Instability," Proceedings of the 2nd International Conference on Vibrations in Rotating Machinery (ImechE), #C306/80, pp. 369-373.

Patankar, S. V., 1980, Numerical Heat Transfer And Fluid Flow, Hemisphere Publishing Corporation, McGraw-Hill.

Pollmann, E., and Termuehlen, H., 1975, "Turbine Rotor Vibrations Excited by Steam Forces (Steam Whirl)," ASME Paper 75-WA/PWR-11.

Ransom, D. L., 1997, "Identification of Dynamic Force Coefficients of a labyrinth and Gas Damper Seal Using Impact Load Excitations," Master's Thesis, Texas A&M University, December.

Richards, R. L., Vance, J. M., and Zeidan, F. Y., 1995, "Using A Damper Seal to Eliminate Subsynchronous Vibrations in Three Back-to-Back Compressors," Proceedings of 24th Turbomachinery Symposium, Houston, September, pp. 59-71.

San Andrés, L., 1991, "Analysis of Variable Fluid Properties, Turbulent Annular Seals," ASME *Journal of Tribology*, Vol. 113, pp. 694-702.

Scharrer, J. K.,1988, "Theory Versus Experiment for the Rotordynamic Coefficient of Labyrinth Gas Seals: Part I - A Two Control Volume Model", ASME Journal of Vibration, Acoustic, Stress, and Reliability in Design, Vol.110, pp. 270-280.

Van Doormaal, J. P., and Raithby, G. D., 1984, "Enhancements of the SIMPLE Method for Predicting Incompressible Fluid Flows," Numerical Heat Transfer, Vol. 7, pp. 147-163.

Vance, J. M., and Li, J., 1996, "Test Results of A New Damper Seal for Vibration Reduction in Turbomachinery," *ASME Journal of Engineering for Gas Turbines and Power*,

Vol. 118, pp. 843-846.

Vance, J. M., and Schultz, R. R., 1993, "A New Damper Seal for Turbomachinery," in Vibration of Rotating System, *Proceedings of the 14th Vibration and Noise Conference*, Albuquerque, New Mexico, ASME DE-Vol. 60, pp. 139-148.

Vance, J. M., and Sundararajan, P., 1993, "Design And Applications Analysis of A New Damper Seal," TRC-Seal-4-93, Turbomachinery Laboratory Research Progress Report, Texas A&M University, College Station, April.

Vance, J. M., Zierer, J. J., and Conway, E. M., 1993a, "Effect of Straight Through Labyrinth Seals on Rotordynamics," Vibration of Rotating Systems, *Proceedings of the 14th Vibration and Noise Conference*, Albuquerque, New Mexico, ASME DE-Vol. 60, pp. 159-171.

Vance, J. M., Cardon, B. P., San Andrés, L. A., and Storace, A. F., 1993b, "A Gas-Operated Bearing Damper for Turbomachinery," *ASME Journal of Engineering for Gas Turbines and Power*, Vol. 115, pp. 383-389.

Wyssmann, H. R., Pham, T. C. and Jenny, R. J., 1984, "Prediction of Stiffness and Damping Coefficients for Centrifugal Compressor Labyrinth Seals," ASME Paper # 84-GT-86.

Yang, Z., San Andrés, L., and Childs, D. W., 1994, "Dynamic Forces Performance of Annular Gas Seals at Off-Center Conditions," STLE *Tribology Transactions*, Vol. 37, 1, pp. 33-44.

Yu, Z., and Childs, D. W., 1997, "A Comparison of Experimental Rotordynamic Coefficients and Leakage Characteristics Between Hole-Pattern Gas Damper Seals and A Honeycomb Seal," ASME Paper 97-GT-9.

Zhou, R. M., 1986, "Instability of Multistage Compressor K1501," *Proceeding of Workshop on Rotordynamic Instability Problems in High-Performance Turbomachinery*, Texas A&M University, NASA CP # 2443, pp. 63-75.

APPENDIX A

COEFFICIENTS FOR FIRST-ORDER BULK-FLOW EQUATIONS

The following coefficients arise from the perturbation of the empirical axial leakage terms and turbulent shear stress terms in the governing equations (18-20 and 23-24). For convenience, the subscript "0" is omitted for all the zeroth-order variables, and the over bar "–" to indicate non-dimensional values is also omitted in the following equations. The subscript "*i*" indicates the variables of the i_{th} axial cavity within the seal.

Continuity and Axial Mass Flow Rate Equations

$$\eta_{mhi} = \zeta\,(\eta_{hbi} - \eta_{hsi})\,; \quad \eta_{mpi} = \zeta\,(\eta_{pbi} - \eta_{psi}) \tag{A.1}$$

$$\eta_{mpui} = -\zeta\eta_{pui}\,; \qquad \eta_{mpdi} = \zeta\eta_{pdi+1} \tag{A.2}$$

where

$$\eta_{hsi} = \eta_{hi}\,; \qquad \eta_{hbi} = \eta_{hi+1} \tag{A.3}$$

$$\eta_{psi} = \eta_{pdi}\,; \qquad \eta_{pbi} = \eta_{pui+1} \tag{A.4}$$

$$\eta_{pdi} = \left(H\mu_c C_{fd}\right)_i / V_*\,; \quad \eta_{pui} = \left(H\mu_c C_{fu}\right)_i / V_* \tag{A.5}$$

$$\eta_{hi} = \left(\mu_f D_p C_{hc}\right)_i / V_* \tag{A.6}$$

$$C_{fui} = \left(\mu_f b_{pu} + D_p a_{fu}\right)_i\,; \qquad C_{fdi} = \left(\mu_f b_{pd} + D_p a_{fd}\right)_i \tag{A.7}$$

$$C_{hci} = \left(Ha_c + \mu_c a_h\right)_i\,; \qquad D_{pi} = \sqrt{P_{i-1}^2 - b_c P_i^2} \tag{A.8}$$

$b_c = 1$ for unchoked flow and $b_c = 0$ for choked flow.

$$b_{pui} = \frac{\partial D_{pi}}{\partial P_{i-1}}\,; \quad b_{pdi} = \frac{\partial D_{pi}}{\partial P_i}\,; \quad a_{fdi} = \frac{\partial \mu_{fi}}{\partial P_i}\,; \quad a_{fui} = \frac{\partial \mu_{fi}}{\partial P_{i-1}} \tag{A.9}$$

$a_{hi} = 1$ for variable clearance and $a_{hi} = 0$ for fixed clearance.

$a_{ci} = a_{hi}\dfrac{\partial \mu_{ci}}{\partial H_i}$ for other teeth and $a_{ci} = 0$ for the first tooth.

Note that μ_f and μ_c are the flow coefficient and "carry-over" factor, respectively, as defined by Childs (1993).

Circumferential Momentum Equation

$$\eta_{xui} = \left(\gamma_{xu} + \gamma_{xx}(\eta_r b_{ru} + \eta_s b_{su}) + \gamma_{xJ} b_{ru}\zeta_r\right)_i \tag{A.10}$$

$$\eta_{xhi} = \left(\gamma_{xD}\gamma_{Dh} + \gamma_{xx}(\eta_r b_{rh} + \eta_s b_{sh}) + \gamma_{xJ} b_{rh}\zeta_r\right)_i \tag{A.11}$$

$$\eta_{xpi} = \left(\gamma_{xx}(\eta_r b_{rp} + \eta_s b_{sp}) + \gamma_{xJ} b_{rp}\zeta_r\right)_i \tag{A.12}$$

$$\eta_{xpui} = \left(\gamma_{xx}(\eta_r b_{rpu} + \eta_s b_{spu}) + \gamma_{xJ} b_{rpu}\zeta_r\right)_i \tag{A.13}$$

$$\eta_{uui} = \zeta \dot{m}_{i+1}; \quad \eta_{uuui} = \zeta \dot{m}_i \tag{A.14}$$

$$\eta_{uhi} = \zeta(\eta_{hbi} U_i - \eta_{hsi} U_{i-1}) \tag{A.15}$$

$$\eta_{upi} = \zeta(\eta_{pbi} U_i - \eta_{psi} U_{i-1}) \tag{A.16}$$

$$\eta_{upui} = \eta_{mpui} U_{i-1}; \qquad \eta_{updi} = \eta_{mpdi} U_i \tag{A.17}$$

$$\eta_{ri} = \frac{1}{2}\zeta_r; \qquad \eta_{si} = \frac{(\zeta_s L_i + B_i + B_{i+1})}{2L_i} \tag{A.18}$$

$$\gamma_{xxi} = \frac{\partial(\Delta\tau_{xi})}{\partial k_{xi}} = -\left(\frac{\mu L U}{D_h}\right)_i; \qquad \gamma_{xDi} = \frac{\partial(\Delta\tau_{xi})}{\partial D_{hi}} = -\left(\frac{\mu L}{D_h^2}\left[k_x U - k_J \frac{\Omega R_r}{2}\right]\right)_i \tag{A.19}$$

$$\gamma_{xJi} = \frac{\partial(\Delta\tau_{xi})}{\partial k_{Ji}} = -\left(\frac{\mu L}{D_h}\frac{\Omega R_r}{2}\right)_i; \qquad \gamma_{xui} = \frac{\partial(\Delta\tau_{xi})}{\partial U_i} = -\left(\frac{\mu L k_x}{D_h}\right)_i \tag{A.20}$$

$$b_{rui} = \gamma_{rui}\left(\mathrm{Re}_r \frac{\partial f_r}{\partial \mathrm{Re}_r} + f_r\right)_i; \qquad b_{sui} = \gamma_{sui}\left(\mathrm{Re}_s \frac{\partial f_s}{\partial \mathrm{Re}_s} + f_s\right)_i \tag{A.21}$$

$$b_{rpi} = a_{rpi}\left(\mathrm{Re}_r \frac{\partial f_r}{\partial \mathrm{Re}_r} + f_r\right)_i; \qquad b_{spi} = a_{spi}\left(\mathrm{Re}_s \frac{\partial f_s}{\partial \mathrm{Re}_s} + f_s\right)_i \tag{A.22}$$

$$b_{rhi} = \left(\mathrm{Re}_r \frac{\partial f_r}{\partial H}\right)_i + a_{rhi}\left(\mathrm{Re}_r \frac{\partial f_r}{\partial \mathrm{Re}_r} + f_r\right)_i \tag{A.23}$$

$$b_{shi} = \left(\mathrm{Re}_s \frac{\partial f_s}{\partial H}\right)_i + a_{shi}\left(\mathrm{Re}_s \frac{\partial f_s}{\partial \mathrm{Re}_s} + f_s\right)_i \tag{A.24}$$

$$a_{rhi} = \left(\gamma_{rD}\gamma_{Dh} + \gamma_{rw}\gamma_{wm}\eta_{hs} + \gamma_{rw}\gamma_{wh}\right)_i \tag{A.25}$$

$$a_{rpi} = \left(\gamma_{rp} + \gamma_{rw}\gamma_{wm}\eta_{ps} + \gamma_{rw}\gamma_{wp}\right)_i \tag{A.26}$$

$$a_{shi} = \left(\gamma_{sD}\gamma_{Dh} + \gamma_{sw}\gamma_{wm}\eta_{hs} + \gamma_{sw}\gamma_{wh}\right)_i \tag{A.27}$$

$$a_{spi} = \left(\gamma_{sp} + \gamma_{sw}\gamma_{wm}\eta_{ps} + \gamma_{sw}\gamma_{wp}\right)_i \tag{A.28}$$

$$\gamma_{rui} = \left.\frac{\partial \mathrm{Re}_r}{\partial U}\right)_i; \qquad \gamma_{rpi} = \left.\frac{\partial \mathrm{Re}_r}{\partial P}\right)_i; \qquad \gamma_{rDi} = \left.\frac{\partial \mathrm{Re}_r}{\partial D_h}\right)_i; \qquad \gamma_{rwi} = \left.\frac{\partial \mathrm{Re}_r}{\partial W}\right)_i \tag{A.29}$$

$$\gamma_{sui} = \left.\frac{\partial \mathrm{Re}_s}{\partial U}\right)_i; \qquad \gamma_{spi} = \left.\frac{\partial \mathrm{Re}_s}{\partial P}\right)_i; \qquad \gamma_{sDi} = \left.\frac{\partial \mathrm{Re}_s}{\partial D_h}\right)_i; \qquad \gamma_{swi} = \left.\frac{\partial \mathrm{Re}_s}{\partial W}\right)_i \tag{A.30}$$

$$\gamma_{wmi} = \left.\frac{\partial W}{\partial \dot{m}}\right)_i; \qquad \gamma_{whi} = \left.\frac{\partial W}{\partial H}\right)_i; \qquad \gamma_{wpi} = \left.\frac{\partial W}{\partial P}\right)_i; \qquad \gamma_{Dhi} = \left.\frac{\partial D_h}{\partial H}\right)_i \tag{A.31}$$

Flow Equations at Radial Baffles

$$\beta_{jpui} = \left(\frac{\partial P_j(\beta)}{\partial P_u}\right)_i; \qquad \beta_{jpdi} = \left(\frac{\partial P_j(\beta)}{\partial P_d}\right)_i \tag{A.32}$$

$$\begin{aligned}
\alpha_{jhi} &= \left(\gamma_{jhw} + \gamma_{jhr} + \gamma_{jhs}\right)_i / \left[1 - \left(\gamma_{jur} + \gamma_{jus} + \gamma_{juw}\right)_i\right] \\
\alpha_{jpui} &= \left(\gamma_{jpuw} + \gamma_{jpur} + \gamma_{jpus}\right)_i / \left[1 - \left(\gamma_{jur} + \gamma_{jus} + \gamma_{juw}\right)_i\right] \\
\alpha_{jpd} &= \left(\gamma_{jpdw} + \gamma_{jpdr} + \gamma_{jpds}\right)_i / \left[1 - \left(\gamma_{jur} + \gamma_{jus} + \gamma_{juw}\right)_i\right]
\end{aligned} \tag{A.33}$$

where

$$\gamma_{juri} = \left(\gamma_{arkr}b_{ru} + \gamma_{arks}b_{su}\right)_{wi}\left(\frac{\Omega R_r}{2}\right)$$

$$\gamma_{jusi} = U_s\left(\gamma_{askr}b_{ru} + \gamma_{asks}b_{su}\right)_{wi} \tag{A.34}$$

$$\gamma_{juwi} = \left(\gamma_{awkr}b_{ru} + \gamma_{awks}b_{su}\right)_{wi}\left(\frac{D_h(P_u - P_d)}{\mu}\right)_{wi}$$

$$\gamma_{jhri} = \left(\gamma_{arkr}b_{rh} + \gamma_{arks}b_{sh} + \gamma_{arDh}\gamma_{Dh} + \gamma_{armb}\eta_{hb}\right)_{wi}\left(\frac{\Omega R_r}{2}\right)$$

$$\gamma_{jhsi} = U_s\left(\gamma_{askr}b_{rh} + \gamma_{asks}b_{sh} + \gamma_{asDh}\gamma_{Dh} + \gamma_{asmb}\eta_{hb}\right)_{wi} \tag{A.35}$$

$$\gamma_{jhwi} = \left(\alpha_w\gamma_{Dh} + D_h\left(\gamma_{awkr}b_{rh} + \gamma_{awks}b_{sh} + \gamma_{awDh}\gamma_{Dh} + \gamma_{awmb}\gamma_{hb} + \gamma_{awh}\right)\right)_{wi}\left(\frac{D_h(P_u - P_d)}{\mu}\right)_{wi}$$

$$\gamma_{jpri} = \left(\gamma_{arkr} b_{rp} + \gamma_{arks} b_{sp} + \gamma_{armb} \eta_{pu}\right)_{wi}$$
$$\gamma_{jpsi} = \left(\gamma_{askr} b_{rp} + \gamma_{asks} b_{sp} + \gamma_{asms} \eta_{pd} + \gamma_{asmb} \eta_{pu}\right)_{wi} \qquad \text{(A.36)}$$
$$\gamma_{jpwi} = \left(\gamma_{awkr} b_{rp} + \gamma_{awks} b_{sp} + \gamma_{awmb} \eta_{pu}\right)_{wi}$$

$$\gamma_{jpuri} = \gamma_{jpri} \beta_{jpui}; \qquad \gamma_{jpdri} = \gamma_{jpri} \beta_{jpdi}$$
$$\gamma_{jpusi} = \gamma_{jpsi} \beta_{jpui}; \qquad \gamma_{\text{jpds}} = \gamma_{\text{jps}} \beta_{\text{jpd}} \qquad \text{(A.37)}$$

$$\gamma_{jpuwi} = \left[\alpha_w + (P_u - P_d)\gamma_{jpw} \beta_{jpu}\right]\left(\frac{D_h}{\mu}\right)_{wi}$$
$$\gamma_{jpdwi} = \left[-\alpha_w + (P_u - P_d)\gamma_{jpw} \beta_{jpd}\right]\left(\frac{D_h}{\mu}\right)_{wi} \qquad \text{(A.38)}$$

$$\gamma_{arkri} = \left.\frac{\partial \alpha_r}{\partial k_r}\right)_i; \qquad \gamma_{arksi} = \left.\frac{\partial \alpha_r}{\partial k_s}\right)_i; \qquad \gamma_{arDhi} = \left.\frac{\partial \alpha_r}{\partial D_h}\right)_i \qquad \text{(A.39)}$$
$$\gamma_{armbi} = \left.\frac{\partial \alpha_r}{\partial \dot{m}_b}\right)_i$$

$$\gamma_{askri} = \left.\frac{\partial \alpha_s}{\partial k_r}\right)_i; \qquad \gamma_{asksi} = \left.\frac{\partial \alpha_s}{\partial k_s}\right)_i; \qquad \gamma_{asDhi} = \left.\frac{\partial \alpha_s}{\partial D_h}\right)_i \qquad \text{(A.40)}$$
$$\gamma_{asmbi} = \left.\frac{\partial \alpha_s}{\partial \dot{m}_b}\right)_i; \qquad \gamma_{asmsi} = \left.\frac{\partial \alpha_s}{\partial \dot{m}_s}\right)_i$$

$$\gamma_{awkri} = \left.\frac{\partial \alpha_w}{\partial k_r}\right)_i; \qquad \gamma_{awksi} = \left.\frac{\partial \alpha_w}{\partial k_s}\right)_i; \qquad \gamma_{awDhi} = \left.\frac{\partial \alpha_w}{\partial D_h}\right)_i \qquad \text{(A.41)}$$
$$\gamma_{awmbi} = \left.\frac{\partial \alpha_w}{\partial \dot{m}_b}\right)_i; \qquad \gamma_{awhi} = \left.\frac{\partial \alpha_w}{\partial H_w}\right)_i$$

APPENDIX B

ZEROTH-ORDER BULK-FLOW ALGEBRAIC EQUATIONS

For convenience, the subscript "0" is omitted for all the zeroth-order variables, and the over bar "–" to indicate non-dimensional values is also omitted in the following equations. The subscript "*i*" indicates the variables of the i_{th} axial cavity within the seal.

B.1 Dimensionless Circumferential Momentum Equation:

For convenience, the diagram of staggered grids (Figure 7) in section 3 is shown here again. Integration of the circumferential momentum equation (29) in the circumferential velocity control volume (U - CV) is expressed as follow:

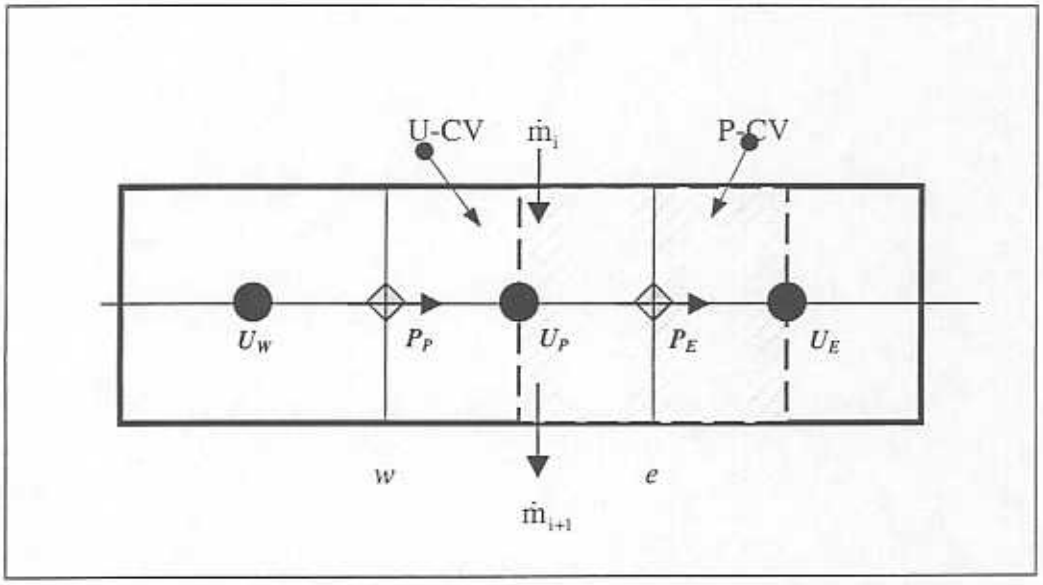

$$\int_w^e a_i \frac{\partial(PU^2)_i}{R_a \partial\Theta} d\Theta + \int_w^e (b_{bi} U_i - b_{ai} U_{i-1}) d\Theta = -\int_w^e a_i \frac{\partial P_i}{\partial\Theta} d\Theta - \int_w^e (d_{ai} U_i - d_{fi}) d\Theta \qquad \text{(B.1)}$$

where

$$a_i = \mathrm{Re}_c \frac{A_i}{R_a} ;$$

$$b_{si} = \dot{m}_i \mathrm{Re}_a ; \qquad b_{bi} = \dot{m}_{i+1} \mathrm{Re}_a ; \tag{B.2}$$

$$d_{xi} = \frac{\mu L_i}{D_{hi}} k_{xi} ; \qquad d_{Ji} = \frac{\mu L_i}{D_{hi}} \frac{\Lambda}{2} k_{Ji}$$

Evaluation of each term in the integral equation above gives,

$$-\int_w^e a_i \frac{\partial P_i}{\partial \Theta} d\Theta = -a_i (P_{ie} - P_{iw}) = a_i (P_{iP} - P_{iE}) \tag{B.3}$$

The second integral on the LHS can be approximately expressed as

$$\begin{aligned} \int_w^e (b_{bi} U_i - b_{si} U_{i-1}) d\Theta &= \int_w^e (b^u_{biP} U_{iP} - b^u_{siP} U_{i-1P}) d\Theta \\ &= b^u_{biP} U_{iP} \delta \Theta^u_P - b^u_{siP} U_{i-1P} \delta \Theta^u_P \end{aligned} \tag{B.4}$$

Similarly, the second integral on the RHS over the U-CV is

$$\begin{aligned} -\int_w^e (d_{xiP} U_i - d_{Ji}) d\Theta &= -\int_w^e (d_{xiP} U_{iP} - d_{JiP}) d\Theta \\ &= -d_{xiP} U_{iP} \delta \Theta^u_P + d_{JiP} \delta \Theta^u_P \end{aligned} \tag{B.5}$$

i.e. where it is assumed that $U_i = U_{iP}$, $b_{bi} = (b_{biP})^u$, $b_{si} = (b_{siP})^u$, $d_{xi} = d_{xiP}$, $d_{Ji} = d_{JiP}$, and an average pressure $P_i = (P_{iP} + P_{iE})/2$ prevails over the U-CV for these two terms. b_{biP} , b_{siP} , d_{xiP} , d_{JiP} are calculated with the average value of pressure on the CV.

$$\int_w^e a_i \frac{\partial (PU^2)_i}{\partial \Theta} d\Theta = a_i (PU^2)_{ie} - a_i (PU^2)_{iw} = a_i P_{iE} U^2_{ie} - a_i P_{iP} U^2_{iw} \tag{B.6}$$

The first integral on the LHS is an advection term (momentum flux). Setting the momentum fluxes as

$$F^u_{ie} = a_i P_{iE} U_{ie} \; ; \quad F^u_{iw} = a_i P_{iP} U_{iw} \tag{B.7}$$

then,

$$\int_w^e a_i \frac{\partial (PU^2)_i}{\partial \Theta} d\Theta = F^u_{ie} U_{ie} - F^u_{iw} U_{iw} \tag{B.8}$$

Note that in the equation above, F_e^u and F_w^u at the faces of the U-CV would require an appropriate interpolation. Typically, advection terms are treated using the upwind scheme that determines the value of the face flow velocity based on whether the flow is into or out of the U-CV. Therefore,

$$\int_w^e a_i \frac{\partial (PU^2)_i}{\partial \Theta} d\Theta = \left\| F^u_{ie}, 0 \right\| U_{iP} - \left\| - F^u_{ie}, 0 \right\| U_{iE} - \left\| F^u_{iw}, 0 \right\| U_{iW} + \left\| - F^u_{iw}, 0 \right\| U_{iP} \tag{B.9}$$

The equation above uses the following algebraic operator definition:

$$\left\| A, \quad B \right\| = \begin{cases} A & \text{if} \quad (A \geq B) \\ B & \text{if} \quad (A < B) \end{cases} \tag{B.10}$$

Substituting the above integral formulae into the momentum integration equation yields,

$$\begin{aligned} &\left\| F^u_{ie}, 0 \right\| U_{iP} - \left\| - F^u_{ie}, 0 \right\| U_{iE} - \left\| F^u_{iw}, 0 \right\| U_{iW} + \left\| - F^u_{iw}, 0 \right\| U_{iP} \\ &+ b^u_{biP} U_{iP} \delta \Theta^u_P - b^u_{iiP} U_{i-1P} \delta \Theta^u_P = a_i (P_{iP} - P_{iE}) - d_{xiP} U_{iP} \delta \Theta^u_P + d_{JiP} \delta \Theta^u_P \end{aligned} \tag{B.11}$$

Rearranging the above equation renders the following discrete circumferential momentum equation:

$$a^u_{iP} U_{iP} = a^u_{iE} U_{iE} + a^u_{iW} U_{iW} + s^u_{iP} + a_i (P_{iP} - P_{iE}) \qquad \text{(B.12)}$$

where

$$\begin{aligned} a^p_{iE} &= \left\| - F^u_{ie}, 0 \right\| \\ a^p_{iW} &= \left\| F^u_{iw}, 0 \right\| \\ a^u_{iP} &= \left\| F^u_{ie}, 0 \right\| + \left\| - F^u_{iw}, 0 \right\| + b^u_{biP} \delta \Theta^u_P + d_{xiP} \delta \Theta^u_P \\ &= a^u_{iE} + a^u_{iW} + F^u_{ie} - F^u_{iw} + b^u_{biP} \delta \Theta^u_P + d_{xiP} \delta \Theta^u_P \\ s^u_{iP} &= b^u_{siP} U_{i-1P} \delta \Theta^u_P + d_{JiP} \delta \Theta^u_P \end{aligned} \qquad \text{(B.13)}$$

Furthermore, in order to smooth convergence, the following under-relaxation formulation is introduced in the equation above with α_u(<1.0) as follows:

$$a^u_{iP} U_{iP} = \alpha_u \left[a^u_{iE} U_{iE} + a^u_{iW} U_{iW} + s^u_{iP} + a_i (P_{iE} - P_{iW}) \right] + (1 - \alpha_u) a^u_{iP} U^{old}_{iP} \qquad \text{(B.14)}$$

The resulting discretized equation is the final form used for the transport of circumferential momentum.

B. 2 Dimensionless Velocity Correction Equation:

For an initial guessed pressure field P^*, a velocity field U^* is calculated from (B.14). Suppose the correct pressure field is expressed as $P = P^* + P'$, then the corresponding velocity can be written as $U = U^* + U'$, and where P' and U' are correction fields. Substituting P and U into the discretized circumferential momentum equation (B.14) yields,

$$\begin{aligned} a^u_{iP} (U^*_{iP} + U'_{iP}) = \alpha_u \left[a^u_{iE} (U^*_{iE} + U'_{iE}) + a^u_{iW} (U^*_{iW} + U'_{iW}) + s^u_{iP} \right] \\ + \alpha_u a_i \left[(P^*_{iP} + P'_{iP}) - (P^*_{iE} + P'_{iE}) \right] + (1 - \alpha_u) a^u_{iP} U^{old}_{iP} \end{aligned} \qquad \text{(B.15)}$$

expanding the equation above yields,

$$a^u_{iP} U'_{iP} = \alpha_u (a^u_{iE} U'_{iE} + a^u_{iW} U'_{iW}) + \alpha_u a_i (P'_{iP} - P'_{iE}) \qquad \text{(B.16)}$$

The *SIMPLEC* procedure (Van Doormaal and Raithby, 1984) approximately sets $U_{iE}'=U_{iW}'=U_{iP}'$ in the equation above, therefore the velocity correction of U_{iP}' is obtained as,

$$U'_{iP} = \frac{\alpha_u a_i (P'_{iP} - P'_{iE})}{a^u_{iP} - \alpha_u (a^u_{iE} + a^u_{iW})} = D^u_{iP} (P'_{iP} - P'_{iE}) \qquad \text{(B.17)}$$

where

$$D^u_{iP} = \frac{\alpha_u a_i}{a^u_{iP} - \alpha_u (a^u_{iE} + a^u_{iW})} \qquad \text{(B.18)}$$

B.3 Dimensionless Pressure Correction Equation

Integration of the continuity equation (22) on the Pressure Control Volume (P - CV) is given as:

$$\int_w^e c_i \frac{\partial (PU)_i}{\partial \Theta} d\Theta + \int_w^e \zeta (\dot{m}_{i+1} - \dot{m}_i) d\Theta = 0 \qquad \text{(B.19)}$$

where

$$c_i = A_i / R_a \qquad \text{(B.20)}$$

The first integral on the LHS renders a mass flux difference as,

$$\int_w^e c_i \frac{\partial (PU)_i}{\partial \Theta} d\Theta = c_i P_{ie} U_{ie} - c_i P_{iw} U_{iw} = c_i P_{ie} U_{iP} - c_i P_{iw} U_{iW} \qquad \text{(B.21)}$$

The second integral is expressed as

$$\int_{w}^{e} \zeta(\dot{m}_{i+1} - \dot{m}_i)d\Theta = \zeta\delta\Theta_P^p(\dot{m}_{i+1P} - \dot{m}_{iP})$$
$$= \zeta\delta\Theta_P^p\left[(\mu_c\mu_f H)_{i+1}\sqrt{P_{iP}^2 - P_{i+1P}^2} - (\mu_c\mu_f H)_i\sqrt{P_{i-1P}^2 - P_{iP}^2}\right] \quad \text{(B.22)}$$

where it is assumed that P_{iP} prevails over the differential P-CV. Substituting the above integration results into Equation (B.19) yields,

$$c_i(P_{ie}U_{iP} - P_{iw}U_{iW}) + \zeta\delta\Theta_P^p\left[(\mu_c\mu_f H)_{i+1}\sqrt{P_{iP}^2 - P_{i+1P}^2} - (\mu_c\mu_f H)_i\sqrt{P_{i-1P}^2 - P_{iP}^2}\right] = 0 \quad \text{(B.23)}$$

Substitution of $P = P^* + P'$ and the corresponding velocity $U = U^* + U'$ into the above equation leads to

$$c_i\left[P_{ie}^*U_{iP}^* + U_{iP}^*P'_{ie} + P_{ie}^*U'_{iP} - P_{iw}^*U_{iW}^* - U_{iW}^*P'_{iw} - P_{iw}^*U'_{iW}\right] + (d_{iP}^* + d_{iP}^pP'_{iP}) = 0 \quad \text{(B.24)}$$

where

$$d_{iP}^* = \zeta\delta\Theta_P^p\left[(\mu_c\mu_f H)_{i+1}\sqrt{P_{iP}^{*2} - P_{i+1P}^{*2}} - (\mu_c\mu_f H)_i\sqrt{P_{i-1P}^{*2} - P_{iP}^{*2}}\right]$$
$$= (b_{biP}^p - b_{siP}^p)\delta\Theta_P^p \quad \text{(B.25)}$$

$$d_{iP}^p = \zeta\delta\Theta_P^p\left((\mu_c\mu_f H)_{i+1}\left[1 - \left(\frac{P_{i+1P}^*}{P_{iP}^*}\right)^2\right]^{\frac{1}{2}} + (\mu_c\mu_f H)_i\left(\frac{P_{iP}^*}{P_{i-1P}^*}\right)\left[1 - \left(\frac{P_{iP}^*}{P_{i-1P}^*}\right)^2\right]^{\frac{1}{2}}\right) \quad \text{(B.26)}$$
$$= b_{biP}^p\frac{P_{iP}^*}{P_{iP}^{*2} - P_{i+1P}^{*2}} + b_{siP}^p\frac{P_{iP}^*}{P_{i-1P}^{*2} - P_{iP}^{*2}}$$

Substitution of $U'_{iP} = D^u_{iP}(P'_{iP} - P'_{iE})$ and $U'_{iW} = D^u_{iW}(P'_{iW} - P'_{iP})$ into the equation above and treating the $(U^*_{iP}P'_{ie})$ and $(U^*_{iW}P'_{iw})$ terms with an upwind scheme yields,

$$c_i\begin{bmatrix}\left(\left\|U^*_{iP},0\right\|+\left\|-U^*_{iW},0\right\|++P^*_{ie}D^u_{iP}+P^*_{iw}D^u_{iW}\right)P'_{iP}-\left(\left\|-U^*_{iP},0\right\|+P^*_{ie}D^u_{iP}\right)P'_{iE}\\ -\left(\left\|U^*_{iW},0\right\|+P^*_{iw}D^u_{iW}\right)P'_{iW}-(P^*_{iw}U^*_{iW}-P^*_{ie}U^*_{iP})\end{bmatrix}+\left(d^*_{iP}+d^P_{iP}P'_{iP}\right)=0 \quad \text{(B.27)}$$

Rearranging this equation yields the following pressure correction formula,

$$a^P_{iP}P'_{iP} = a^P_{iE}P'_{iE}+a^P_{iW}P'_{iW}+s^P_{iP} \quad \text{(B.28)}$$

where

$$\begin{aligned}
a^P_{iE} &= c_i\left(\left\|-U^*_{iP},0\right\|+P^*_{ie}D^u_{iP}\right)\\
a^P_{iW} &= c_i\left(\left\|U^*_{iW},0\right\|+P^*_{iw}D^u_{iW}\right)\\
a^P_{iP} &= c_i(\left\|U^*_{iP},0\right\|+\left\|-U^*_{iW},0\right\|+P^*_{ie}D^u_{iP}+P^*_{iw}D^u_{iW})+d^P_{iP}\\
&= a^P_{iE}+a^P_{iW}+c_i(U^*_{iP}-U^*_{iW})+d^P_{iP}\\
s^P_{iP} &= c_i(P^*_{iw}U^*_{iW}-P^*_{ie}U^*_{iP})-d^*_{iP}
\end{aligned} \quad \text{(B.29)}$$

APPENDIX C

FIRST-ORDER BULK-FLOW ALGEBRAIC EQUATIONS

For convenience, the subscript "0" is omitted for all the zeroth-order variables, and the over bar "–" to indicate non-dimensional values is also omitted in the following equations. The subscript "i" indicates the variables of the i_{th} cavity within the seal.

C.1 Circumferential Momentum Equation

By substituting the first-order continuity equation (24) into the momentum equation (25), the first-order circumferential momentum equation is further simplified to,

$$\begin{aligned} \mathrm{i}\,\mathrm{Re}_i\left(PAU_j\right)_i + \frac{\mathrm{Re}_c}{R_a}\frac{\partial}{\partial\Theta}\left(PUAU_j\right)_i + \frac{\mathrm{Re}_c}{R_a}\frac{\partial}{\partial\Theta}\left(PAU_j + PULH_j + UAP_j\right)_i\left(\frac{\partial U}{\partial\Theta}\right)_i \\ = -\frac{\mathrm{Re}_c}{R_a}\left(A\frac{\partial P_j}{\partial\Theta}\right)_i + \left(c_{xu}U_j + c_{xh}H_j + c_{xp}P_j\right)_i + c_{xuui}\left(U_j\right)_{i-1} + c_{xpui}\left(P_j\right)_{i-1} \end{aligned} \tag{C.1}$$

where

$$\begin{aligned} \mathrm{i} &= \sqrt{-1} \\ c_{xui} &= \eta_{xui} - \mathrm{Re}_c\,\eta_{uui} \\ c_{xhi} &= \eta_{xhi} - \frac{\mathrm{Re}_c L_i}{R_a}\frac{\partial P_i}{\partial\Theta} + \mathrm{Re}_c U_i\eta_{mhi} - \mathrm{Re}_c\,\eta_{uhi} \\ c_{xpi} &= \eta_{xpi} + \mathrm{Re}_c U_i\eta_{mpi} - \mathrm{Re}_c\,\eta_{upi} \\ c_{xuui} &= \mathrm{Re}_c\,\eta_{uuui} \\ c_{xpui} &= \eta_{xpui} + \mathrm{Re}_c\,\eta_{mpui}\left(U_i - U_{i-1}\right) \end{aligned} \tag{C.2}$$

Integration of equation (C.1) on the velocity control volume (U-CV) yields the following discrete circumferential flow momentum equation:

$$a^u_{jP}U_{jP} = a^u_{jE}U_{jE} + a^u_{jW}U_{jW} + s^u_{jP} + \left(c^u_{jP}P_{jP} - c^u_{jE}P_{jE}\right) \tag{C.3}$$

where

$$a^{p}_{jE} = \left\| -F^{u}_{ie}, 0 \right\| ; \qquad a^{p}_{jW} = \left\| F^{u}_{iw}, 0 \right\| \tag{C.4}$$

$$a^{u}_{jP} = a^{u}_{jE} + a^{u}_{jW} + F^{u}_{ie} - F^{u}_{iw} + a_{xut}\delta\Theta^{u}_{P} \tag{C.5}$$

$$s^{u}_{jP} = a_{xhi}\left(\Phi_{je} - \Phi_{jw}\right) + a_{xuui}\delta\Theta^{u}_{P}\left(U_{j}\right)_{i-1} + a_{xpui}\delta\Theta^{u}_{P}\left(P_{j}\right)_{i-1} \tag{C.6}$$

$$c^{u}_{jP} = a_{i} + \frac{1}{2}a_{xpi}\delta\Theta^{u}_{P} ; \qquad c^{u}_{jE} = a_{i} - \frac{1}{2}a_{xpi}\delta\Theta^{u}_{P} \tag{C.7}$$

$$a_{xui} = \mathrm{i}\,\mathrm{Re}_{t}\,P_{i}A_{i} + \frac{\mathrm{Re}_{c}\,P_{i}A_{i}}{R_{a}}\frac{\partial U_{i}}{\partial\Theta} - c_{xui} ; \qquad \mathrm{i} = \sqrt{-1} \tag{C.8}$$

$$a_{xhi} = c_{xhi} - \frac{\mathrm{Re}_{c}\,P_{i}U_{i}L_{i}}{R_{a}}\frac{\partial U_{i}}{\partial\Theta} \tag{C.9}$$

$$a_{xpi} = c_{xpi} - \frac{\mathrm{Re}_{c}\,U_{i}A_{i}}{R_{a}}\frac{\partial U_{i}}{\partial\Theta} \tag{C.10}$$

$$a_{xuui} = c_{xuui} ; \qquad a_{xpui} = c_{xpui} \tag{C.11}$$

$$\Phi^{u}_{j} = \sin\Theta ; \quad j = X \tag{C.12}$$

$$\Phi^{u}_{j} = \cos\Theta ; \quad j = Y \tag{C.13}$$

C. 2 Dimensionless Pressure Correction Equation

Integration of the continuity equation (22) on the pressure control volume yields the following discrete pressure correction equation:

$$a^{p}_{jP}\,P'_{jP} = a^{p}_{jE}\,P'_{jE} + a^{p}_{jW}\,P'_{jW} + s^{p}_{jP} \tag{C.14}$$

where

$$a^{p}_{jE} = a_{i}\left(\left\| -U_{iP}, 0 \right\| + P_{ie}\,DE^{u}_{jP}\right) \tag{C.15}$$

$$a^{p}_{jW} = a_{i}\left(\left\| U_{iW}, 0 \right\| + P_{iw}\,DP^{u}_{jW}\right) \tag{C.16}$$

$$a^{p}_{jP} = a^{p}_{jE} + a^{p}_{jW} + a_{i}\left(U_{iP} - U_{iW}\right) + a_{mpi}\delta\Theta^{p}_{P} \tag{C.17}$$

$$\begin{aligned} s^{p}_{jP} = {} & a_{i}\left(P_{iw}U^{*}_{jW} - P_{ie}U^{*}_{jP}\right) + a_{i}\left(U_{iW}P^{*}_{jw} - U_{iP}P^{*}_{je}\right) \\ & + b_{i}\left(P_{iw}U_{iW}H_{jw} - P_{ie}U_{iP}H_{je}\right) + a_{mhi}\left(\Phi^{p}_{jw} - \Phi^{p}_{je}\right) \\ & - \left[a_{mpi}P^{*}_{jP} + a_{mpui}\left(P^{*}_{jP}\right)_{i-1} + a_{mpdi}\left(P^{*}_{jP}\right)_{i+1}\right]\delta\Theta^{p}_{P} \end{aligned} \tag{C.18}$$

$$a_i = A_i / R_a \; ; \qquad b_i = L_i / R_a \tag{C.19}$$

$$a_{mhi} = \eta_{mhi} + \mathrm{i}\sigma P_i L_i \; ; \quad a_{mpi} = \eta_{mpi} + \mathrm{i}\sigma A_i \; ; \qquad \mathrm{i} = \sqrt{-1} \tag{C.20}$$

$$a_{mpui} = \eta_{mpui} \; ; \qquad a_{mpdi} = \eta_{mpdi} \tag{C.21}$$

$$DP^u_{jP} = \frac{\alpha_{ju} c^u_{jP}}{a^u_{jP} - \alpha_{ju}(a^u_{jE} + a^u_{jW})} \; ; \qquad DE^u_{jP} = \frac{\alpha_{ju} c^u_{jE}}{a^u_{jP} - \alpha_{ju}(a^u_{jE} + a^u_{jW})} \tag{C.22}$$

APPENDIX D

EXPERIMENTAL INVESTIGATIONS AND THEORETICAL MODELS FOR BRUSH SEALS

Jiming Li, Research Assistant

Brush seals are densely packed beds of directionally compliant bristles clamped between upstream and downstream retainers (plates). The bristles are oriented to the shaft at a lay angle that points in the rotation direction. Ferguson (1988) finds the leakage of the brush seal to be extremely low, only 5% ~ 10%/ that of labyrinth seals, and running in the same turbomachinery with clearances of 0.75 mm.

Over their lifetime, brush seals are subjected to considerable wear and thermal loads. Hence, brush seals usually require a hardened smooth interface. Bristle material and rotor coating become a major design consideration. Typically, the bristles are made of a super alloy, while the rotor is coated with a highly polished ceramic. Another primary limitation on the applications of brush seals is a relatively small pressure drop restriction. Currently this type of seal is ordinarily considered for applications in aeroengines, gas compressors, and steam generators due to the possible degradation of the seal caused by liquid lubricant contamination.

The leakage flow mechanism through the pack of bristles is not yet fully understood. However, various models for the flow through brush seals have been proposed to correlate test data to important parameters. Based on available technical papers, experimental and theoretical investigations into the sealing and rotordynamic characteristics of brush seals are summarized below.

Experimental Investigations on Brush Seals

Chupp and Dowler (1993) investigate the performance of brush seals in limited-life gas turbine engines. Test results show that single-stage brush seals reduce the leakage around 80% when compared to a four-blade labyrinth seal. The leakage rate of brush seals is not sensitive to the pressure ratio (< 3.2) as in the case of labyrinth seals. The authors recommend multiple-stage brush seals in series for decreasing both the leakage and the pressure drop cross each brush stage.

Carlile et al. (1993) show experimentally that brush seals reduce leakage up to 9.5 times when compared to an annular seal. The authors also find a brush seal with reversing pressure drop across the brush seal to produce approximately the same leakage as the annular seal. Therefore, proper installation of brush seals is critical in practice. The effect of a lubricant in the bristle packs is demonstrated to be favorable to further reduce the leakage. The authors perform an analysis to generalize various working fluid data with the Corresponding State Theory. Comparisons show that only the air and carbon dioxide test data correlate well with the model.

Chupp, et al. (1995, 1997) investigate the feasibility to apply brush seals to large utility, industrial size gas turbines. For industrial gas turbines, the wear characteristics of brush seals are most important due to the desired long operating life and large clearance rotor excursions during machine startup. Another constraint, which distinguishes large industrial gas turbines from aerospace engines, is the necessity to run against an uncoated rotor surface. Even a moderate leakage reduction is significant because the clearances of current labyrinth seals are too large. The authors' investigations show that installing brush seals in large utility gas turbine engines can decrease the turbine leakage by one-third and consequently improve plant efficient by one-fourth of a percent.

Leakage Models for Brush Seals

Chupp, et al. (1991) develop a simple leakage flow model to correlate the leakage data throughout a range of test and application conditions. The model introduces a single parameter, the effective brush thickness, to correlate flow through the brush seals for a given configuration and a set of pressure and temperature conditions. The effective brush thickness (B) is a measure of the compactness of the bristle bed. As (B) increases, the bristle pack opens up and the flow leakage increases. Therefore, the effectiveness of the simple model is determined by selecting an accurate effective brush thickness. Chupp and Holle (1996) report a revised model, which can determine more realistic effective thickness based on an hexagonal array of staggered cylinders. A computational procedure to correlate the effective thickness and the leakage is also given in this paper. This model

will be implemented into the leakage program for hybrid brush/labyrinth/damper seals at the Rotordynamic Laboratory.

Hendricks et al. (1991) present a comprehensive bulk-flow model to describe global phenomena across the bristle pack based on the theory of flows in porous media. The comparison to experimental results shows that the model predicts mass flow rate well. However, detailed knowledge of the brush seal is required, and the analysis complexity would appear to make the use of this model unprofitable in most cases. Hendricks et al. (1996) simplify Ergun's porous flow model (Ergun, 1952) to investigate the flow in brush seals. The bristle pack is idealized as a pin array. A quadrilateral grid finite difference scheme is implemented for the FEM-flow solver. The authors find the model predicts leakage and pressure drop well in the laminar flow region.

Chew and Hogg (1997) develop a simple one-dimensional porosity flow model for predicting leakage through the bristle pack of brush seals. Bristle drag is calculated from a linear combination of viscous and inertial fluid flow effects. Comparisons to test data (Carlile, et al., 1993) show that this model predicts brush seal leakage well. Like in Chupp and Holle's model, the dimensionless bristle pack thickness must be determined first from correlations with experimental data.

Sharatchandra and Rhode (1996) investigate numerically the effect of rotor induced swirl on the leakage characteristics of brush seals. Two-dimensional Navier-Stokes equations are solved to obtain the detailed velocity and pressure distributions in the brush seal. The model predicts that the leakage decreases with increasing rotor speeds since leakage resistance is increased. The reliability of the computational model has been demonstrated by comparing to measurements from flows in a tube tank.

Rotordynamic Coefficients of Brush Seals

Experimental results of the dynamic force coefficients for brush seals are limited. Conner and Childs (1990) measure the dynamic force coefficients of a four-stage brush seal and compare its dynamic performance with other labyrinth seals. Test results show that the cross-coupled stiffness for brush seals is small and generally negative. This coefficient appears also insensitive to the flow pre-swirl, indicating that the brushes work

as a seal and a swirl brake. At high rotor speeds, the measured damping values for brush seals are 3~4 times smaller than those from labyrinth seals. The experiments show the brush seal direct stiffness varies with the excitation frequency while the remaining rotordynamic coefficients do not show any frequency dependence. The direct stiffness for the brush seal is positive and slightly increases with an increase in pressure ratio.

Hendricks, et al. (1991) present a simple expression to evaluate the stiffness coefficients of a single-stage brush seal with a cantilevered elastic beam model. The authors demonstrate that the cross-coupled stiffness (k) is always negative, thus making brush seals a stabilizing source in rotor dynamics. However, the friction coefficient in the formulae used is not fully detailed. No comparisons to measured force coefficients are reported.

To date, no computational models have been reported to fully characterize the flow field in a bristle pack, including the determination of rotordynamic coefficients in brush seals.

Computer Program for Brush Seal Leakage

A computer code (Hybrid) is developed for evaluation of the leakage rate of hybrid brush/labyrinth seals. The model combines Chupp and Holle's model (1996) with the labyrinth seal leakage formula (Childs, 1993), The brush can be installed at the inlet or exit plane of the hybrid seals. The geometric and operating parameters are directly read from an input file "labybrush.dat". The following brush seal parameters are required for the analysis:

Bristle diameter: db (in)

Bristle pack density: N (bristles/in)

Rotor diameter: Dj (in)

Diameter of the brush retainer plate: Du (in)

Effective brush thickness: B (in) (based on correlations with test data)

Initial guess of flow factor Φ (nondimension mass flow rate): 0.0015 suggested.

Numerical example: a three-cavity hybrid labyrinth/brush seal (Figure 1) is evaluated. The brush-seal is installed at the seal downstream (discharge plane). The input data are given in Table 1. Numerical results are given in Table 2.

Table 1. Input data of a hybrid laby/brush seal (four teeth)

Seal pitch	7.6 (mm)
Seal clearance (at first three teeth)	0.1016 (mm)
Seal clearance at brush	0.000 (mm)
Inlet pressure	4.135 (bar)
Discharge pressure	1.013 (bar)
Gas temperature	296 (K)
Bristle diameter	0.0028 (in)
Bristle pack density	3500
Rotor diameter	5.10 (in)
Diameter of the brush retainer plate	5.832 (in)
Effective brush thickness	0.03
Initial guess of flow factor	0.0012

Table 2. Pressure distribution and flow factor of a hybrid seal (four teeth)

Ps (bar)	P1(bar)	P2(bar)	P3(bar)	Pb(bar)	Flow factor
4.135	4.016	3.927	3.836	1.013	1.231
P ratio	Ps/P1=1.03	P1/P2=1.023	P3/P2=1.024	P3/Pb=3.787	

Figure 1. Schematic of a three-cavity hybrid Laby/Brush seal.

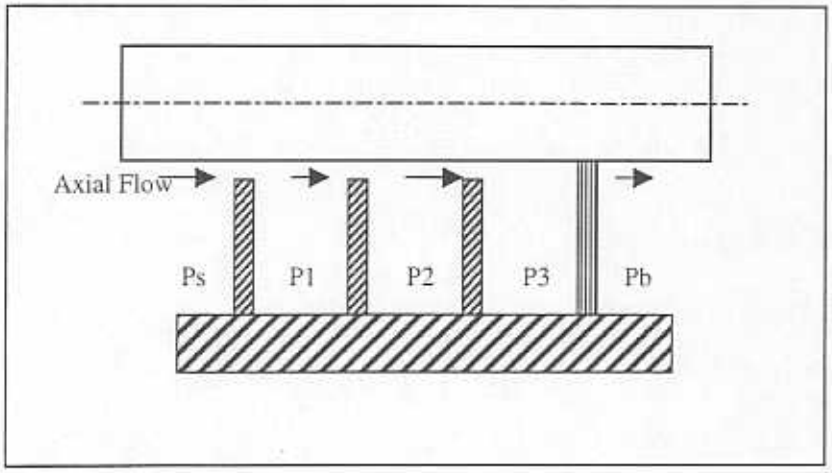

The results given in Table 2 show that the brush seal stage sustains the largest pressure drop. The first two labyrinth cavities act as static gas chambers since only small pressure drops occur across them.

The "brush1" program developed is also used to calculate single-stage brush seal leakage. The results could be validated with the data reported by Chupp and Holle (1996). A comparison between predictions and measurements are shown in Table 3. Input data is detailed in Table 1 of Chupp and Holle (1996).

Table 3. Comparison with measurements for brush seal "CROSSTHK"
At pressure ratio = 4.0 and effective brush thickness = 0.03" **(Chupp and Holle, 1996)**

Flow factor from **code: BRUSH1**	Flow factor measured (Fig. 4)	Minimum brush thickness from **code: BRUSH1**	Minimum brush thickness (Fig.6)
0.00132	0.00125	**0.02876**	0.0287

Recommendations for implementation in a bulk-flow model for hybrid seals

There are three main issues that need to be handled properly in order to implement the brush seal leakage model with the current damper seal computational model:

- The effects of flow in the bristle pack and the thin gas film between bristle tips and rotor surface. A thin gas film most likely exists when the pressure drop across the seal is too large. Probably this effect could be neglected. Furthermore, the bristle pack could be considered as a pure cantilevered elastic beam (Hendricks et al.,1991) from which only stiffness coefficients are evaluated approximately.
- A suitable friction factor for the side surfaces of brush seals is needed. Moody's friction factor model may be appropriate.
- Evaluation of the flow variables (derivatives) in the brush-seal installed at the last cavity is needed for proper derivation of the first-order equations and evaluation of force coefficients. If it is assumed that the axial flow (leakage) through the brush-seal stage is independent of rotor whirl amplitude, then no major difficulty arises because the first-order variables in the last cavity are only determined by the upstream conditions.

In summary, the latest theoretical and experimental investigations on brush seals are discussed as per review of the relevant literature. A computer program for calculation of the leakage of hybrid brush/labyrinth seals is developed and validated with existing test data. Some considerations are discussed for further development of the existing damper seal model if the brush-seal stage is combined with teeth-on-stator labyrinth seals and/or pocket damper seals bulk-flow models.

REFERENCES FOR BRUSH SEALS

Chew, J. W., and Hogg, S. I., 1997, "Porosity Modeling of Brush Seals," ASME Journal of Tribology, Vol. 119, pp. 769-775.

Childs, D. W., 1993, "Turbomachinery Rotordynamics: Phenomena, Modeling, & Analysis," John Wiley & Sons, Inc., New York, pp. 300.

Chupp, R. E., and Dowler, C. A., 1993, "Performance Characteristics of Brush Seals for Limited-Life Engines," ASME Journal of Engineering for Gas Turbines and Power, Vol. 115, pp. 390-396.

Chupp, R. E., Holle, G. F., 1996, "Generalizing Circular Brush Seal Leakage Through a Randomly Distributed Bristle Bed," ASME Journal of Turbomachinery, Vol. 118, pp. 153-161.

Chupp, R. E., and Loewenthal, R. G., 1997, "Brush Seals Can Improve Power Plant Efficiency by One-Fourth of a Percentage Point Yielding Huge Annual Savings," Lubrication Engineering, June, pp. 10-14.

Chupp, R. E., Holle, G. F., and Dowler, C. A., 1991, "Simple Leakage Flow Model for Brush Seals," AIAA 91-1913, AIAA/SAE/ASME 27th Joint Propulsion Conference, June 24-26, Sacramento, CA.

Chupp, R. E., Johnson, R. P., and Loewenthal, R. G., 1995, "Brush Seal Development for Large Industrial Gas Turbines," AIAA 95-3146, AIAA/SAE/ASME/ASEE 31th Joint Propulsion Conference, July 10-12, San Diego, CA.

Conner, K., and Childs, D., 1990, "Rotordynamic Coefficient Test Results for A 4-Stage brush Seal,"" AIAA 90-2139, AIAA/SAE/ASME/ASEE 26th Joint Propulsion Conference, July 16-18, Orlando, FL.

Ergun, S., 1952, Chem Engr. Prog., 43(93).

Ferguson, J. G. 1988, "Brushes as High Performance Gas Turbine Seals", ASME Paper No. 88-GT-182.

Hendricks, R. C., Schlumberger, S., Braun, M. J., Choy, F., and Mullen, R. L., 1991, "A Bulk Flow Model of a Brush Seal System," ASME paper 91-GT-325.

Hendricks, R. C., Kudriavtsev, V.V., Braun, M. J. and Athavale, M. M., 1996, "Flows in Pinned Arrays Simulating Brush Seals," presented at International Congress on Fluid Dynamics and Propulsion, December 29-31.

Sharatchandra, M. C., and Rhode, D. L., 1996, "Computed Effects of Rotor-Induced Swirl on Brush Seal Performance – Part 1: Leakage Analysis," ASME Journal of Tribology, Vol. 118, pp. 912-919.